Factors Influencing Small-Strain Stiffness of soils and its Determination

Term Paper

By
Milad Asslan

2008

Bauhaus-Universität Weimar

Professur Bodenmechanik

Supervisors:
Dr.-Ing. Frank Wuttke
Prof. Dr.-Ing. habil. Tom Schanz
Dr.-Ing. Hans-Gottfried Schmidt

I declare that I wrote this term paper my self and I did not use any other references than those mentioned in this paper.

Milad Asslan

Acknowledgment

I would like to acknowledge and extend my heartfelt gratitude to the following persons, who have made the completion of this term paper possible:

Prof. Dr.-Ing. habil. Tom Schanz for his very valuable suggestions, corrections, and for his careful reviewing of this paper.

Dr.-Ing. Frank Wuttke for his continuous guide through my term paper, for all his suggestions and ideas, and for all the materials he gave me to read.

Dr.-Ing. Hans-Gottfried Schmidt for his advices and for encouraging me.

Table of Content

Table of Figures

Chapter I
Small-Strain Stiffness

1.1 Introduction

The initial shear modulus G_{max} of soil is an important parameter for a variety of geotechnical design applications. This modulus is typically associated with shear strain levels about $5*10^{-3}$% and below. The critical role of soil stiffness at small-strains in the design and analysis of geotechnical infrastructure is now widely accepted.

G_{max} is a key parameter in small-strain dynamics analyses such as those to predict soil behaviour or soil-structure interaction during earthquake, explosions or machine or traffic vibration where it is necessary to know how the shear modulus degrades from its small-strain value as the level of shear strain increases. G_{max} can be equally important for small-strain cyclic situations such as those caused by wind or wave loading and also for small-strain static situations. G_{max} may also be used as an indirect indication of various soil parameters, as it in many cases correlates well to other soil properties such as density and sample disturbance. In recent years, a technique using bender elements was developed to investigate the small-strain shear modulus G_{max}. The value of G_{max} depends on a number of parameters, including void ratio, confining stress, soil structure, degree of saturation, temperature, stress history and time.

1.2 Small-Strain Stiffness

The shear modulus is usually expressed as the secant modulus by the extreme points on the hysteresis loop (Seed & Idriss, 1970) (Figure 1). The first loading curve, sometimes called the backbone curve, connects the load inversion points of oscillation periods with different levels of shear strain and has a hyperbolic shape. The slope in the origin point to this curve corresponds to the shear modulus G_{max} or G_0. The stress-strain relationship in the very small-strain is considered a line; therefore, G_{max} is the shear modulus in the small-strain range, usually assumed at values below the linear elastic threshold strain of about $5*10^{-3}$ %.

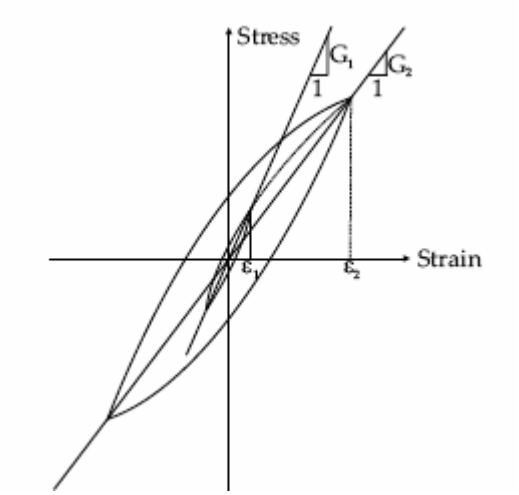

Figure 1. Stress-strain hysteresis loops G2<G1 for ε2 >ε1 (Seed & Idris, 1970)

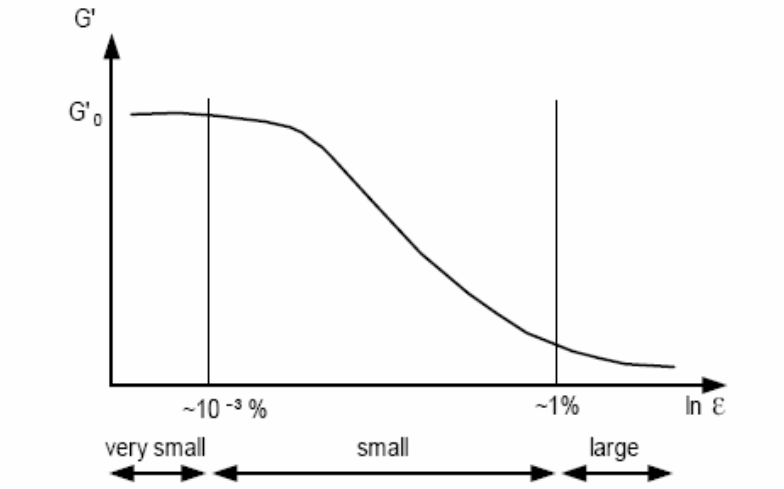

Figure 2. An idealization of the variation of stiffness with strain for soil (Atkinson & Sallfors, 1991)

Figure 2 shows the reduction of stiffness with increment of strain (Atkinson, Sallfors, 1991). It is worthy to say, it is in general expected that G_{max} does not change in the low-strain range.

Figure 3 illustrates typical strain ranges for structures and typical laboratory tests to measure different strains. Vibrations caused by seismic in situ tests, traffic, construction works, weak earthquakes or even blastings usually have shear strain amplitudes below $5*10^{-3}$ %.

(Yamashita et al., 2001) analyzed results of tests from nineteen laboratories done on sand, clay and soft rock. Monotonic tests (triaxial and torsional) and cyclic tests (triaxial, torsional and resonant column) were performed in this international parallel program. They found that stiffness at strains between 10^{-5} and 10^{-3} was similar between monotonic and cyclic tests.

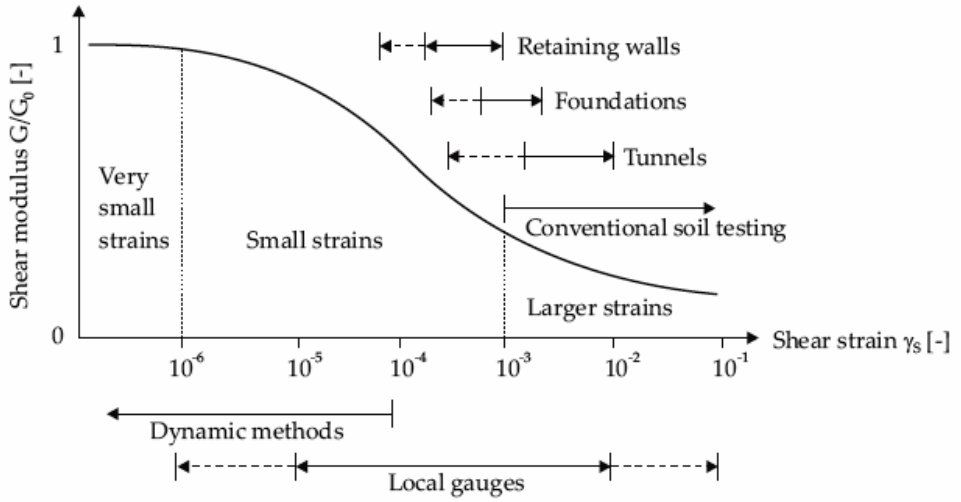

Figure 3. Characteristic stiffness-strain behavior of soil with typical strain ranges for laboratory tests and structures (Atkinson and Sallfors, 1991) and (Mair, 1993)

There are two types of cyclic threshold shear strain, they are the linear cyclic threshold shear strain, γ_{tl}, and the volumetric cyclic threshold shear strain, γ_{tv}, with $\gamma_{tv} > \gamma_{tl}$. These strains represent boundaries between fundamentally different categories of cyclic soil behavior. For cyclic strains below γ_{tl}, soil behaves essentially as a linearly elastic material. Between γ_{tl} and γ_{tv}, soil becomes markedly nonlinear but remains largely elastic because permanent changes of its microstructure still do not occur or are negligible. Above γ_{tv} soil becomes increasingly nonlinear and inelastic, with significant permanent microstructural changes taking place under cyclic loading. That is, γ_{tv} = the threshold separating cyclic strains that cause or do not cause significant permanent changes of soil microstructure. (Vucetic, 1994) identified these two thresholds for different types of soils. He showed how the value of the threshold shear strain depends on soil type. Figure 3 shows that for many different sands γ_{tv} is essentially 10^{-2} %, regardless of confining stress, density, and specimen fabric. Cyclic triaxial strain-controlled test

results obtained for a gravel by (Hynes- Griffin, 1988) showed that γ_{tv} in gravels is affected by initial effective mean normal stress, $\bar{\sigma}_0$ and OCR in the same way, i.e., it increases somewhat with $\bar{\sigma}_0$ and OCR. However, γ_{tv} values obtained by (Hynes-Griffin, 1988) for gravel are generally smaller than for sands, ranging between $0.5*10^{-2}$ % and $2*10^{-2}$ %.

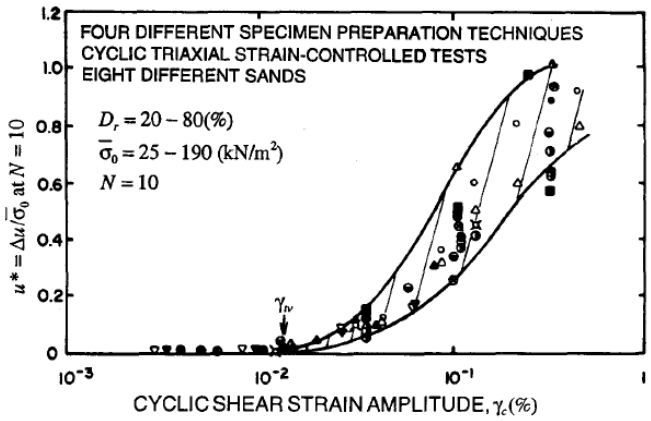

Figure 4. Buildup of Residual Pore-Water Pressure in Different Sands in Cyclic Triaxial Strain-Controlled Tests (Vucetic, 1994).

Based on different researches and on his study, (Vucetic, 1994) concluded that for every soil a cyclic shear strain amplitude can be found below which: (1) There is essentially no permanent microstructural change; (2) residual cyclic pore-water pressure essentially does not develop if the soil is fully saturated and cyclically sheared in undrained conditions; and (3) the permanent volume change is negligible if the soils is dry, partially saturated, or fully saturated with drainage allowed. If during cyclic shearing this threshold cyclic shear strain is exceeded: (1) The microstructure is altered irreversibly; (2) the soil stiffness changes permanently; (3) in fully saturated soils loaded in undrained conditions a permanent cyclic pore-water pressure develops; and (4) in dry, partially saturated, or fully saturated soils with drainage allowed, a permanent volume change accumulates.

(Santos & Gomes Correia, 2001) investigated the shear modulus degradation based on a key parameter defined by them and called reference threshold shear stain, $\gamma_{0.7}$. This parameter is defined as the shear strain for a stiffness degradation factor of G/G_{max}=0.7, in which G_{max} is the very small-strain shear modulus and G is the secant shear modulus. Their approach was the following, to characterize the non-linear secant stiffness of soils, two parameters are needed: G_{max} which defines the rigidity of soil at very small strain; and the reference threshold shear stain, $\gamma_{0.7}$ which characterizes the degree of non-linearity at medium-strain levels.

(Burland, 1989) described soil behaviour at very small strain region. He found that soil exhibits high stiffness at small-strain and non-linear stress-strain response. By studying constructions of practical project, he showed the significant effect of small-strain behaviour on soil-structure interaction, stress distribution in soil mass and displacement profiles around loaded areas and excavation. He also compared laboratory test using LVDTs with in-situ tests at small-strain levels. He found that, if the strains are

measured locally to a high accuracy, tests on high-quality samples at the appropriate confining pressure give remarkably accurate and consistent measurements of the in-situ small-strain stiffness.

(Clayton & Heymann, 2001) the behaviour at very small strains of three widely different natural materials: Bothkennar clay, Londonclay, and a high-porosity Chalk. They used LVDTs to measure small-strain in laboratory. They found that Stiffness measured in the triaxial apparatus at very small strain levels were similar to stiffness obtained using field geophysical techniques. They also found that at very small-strain levels the observed stress-strain behaviour appeared to be linear for all three materials.

(Tatsuoka et al., 2001) achieved a development of a more unified view for static and dynamic behaviour and laboratory and field testing. Figure 5 illustrates a typical example of inconsistency in stress-strain relationship between field tests (PLT: plate load test, PMT: pressuremeter test) and a conventional triaxial compression test (TC). Such low stiffness values obtained from conventional laboratory stress-strain tests were often considered due to serious effects of sample disturbance. Although this effect is still important, it may not be the exclusive cause. It is common to obtain different stiffness values among conventional laboratory stress-strain tests, and also among conventional in-situ tests. Therefore, the link between laboratory stress-strain tests and in-situ tests is missing, in particular among practicing engineers. It is also considered that elastic stiffness from in-situ wave velocity is irrelevant when predicting ground deformation and structural displacements at static loads. It was common to obtain elastic deformation property by performing dynamic tests such as resonant column and wave propagation tests. Later (Shibuya et al., 1992) and (Tatsuoka et al., 1995), among others, showed that the strain rate dependency of the stiffness at small-strain in cyclic torsional shear was very low. (Woods, 1991) and (Tatsouka & Shibuya, 1991) pointed out that it is not necessary to distinguish between dynamically and statically measured elastic stiffness values, when measured under the same conditions. From analyzing significant amount of data, (Tatsuoka et al., 2001) found the same conclusion.

Figure 6 illustrates stress-strain relationship in triaxial compression test measured with external axial gauge and field full scale test on a high-quality sample. It shows that the stiffness in the field is significantly underestimated.

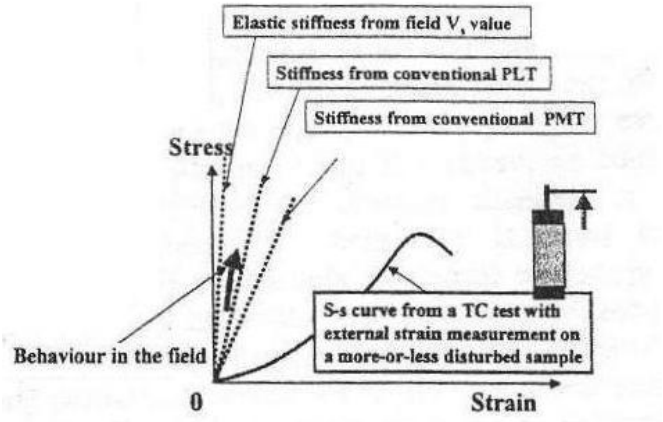

Figure 5. Inconsistent stress-strain behaviour among laboratory and in-situ tests (Tatsuoka et al., 2001).

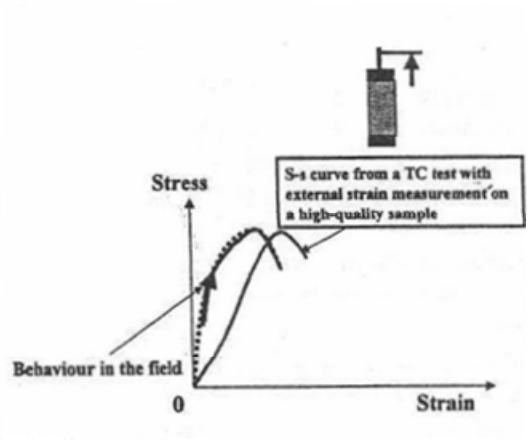

Figure 6. Inconsistent stress-strain behaviour between TC with external axial strain measurement on a high-quality sample and field test (Tatsuoka et al., 2001)

1.3 Effects to Small-Strain Stiffness

Many factors affect the small-strain stiffness and its reduction such as confining stress, void ratio and strain amplitude. Each influence is discussed in this chapter based on a literature review. At the end, a table shows a list of parameters with different level of importance.

1.3.1 The influence of shear strain and volumetric strain

(Lade & Abelev, 2005) studied volumetric stress-strain behaviour of Nevada sand in isotropic compression test as shown in Figure 7. They compared bulk modulus B obtained from isotropic loading and unloading to that obtained from interrupting continues loading process with small load cycles. They found that in primary loading, soil stiffness load cycles is higher than soil stiffness in continues loading. On the other hand, during unloading, load cycles did not show significant stiffness increase. This is also in agreement with the findings of (Zdravkovic & Jardine, 1997). The shear modulus G_{max} can be obtained from E_{max} modulus or B modulus by assuming a value for Poisson's ratio (e.g. Atkinson, 2000), since it is a common simplification to assume that Poisson' ration is constant in the small-strain level, although it increases slightly with applied strain.

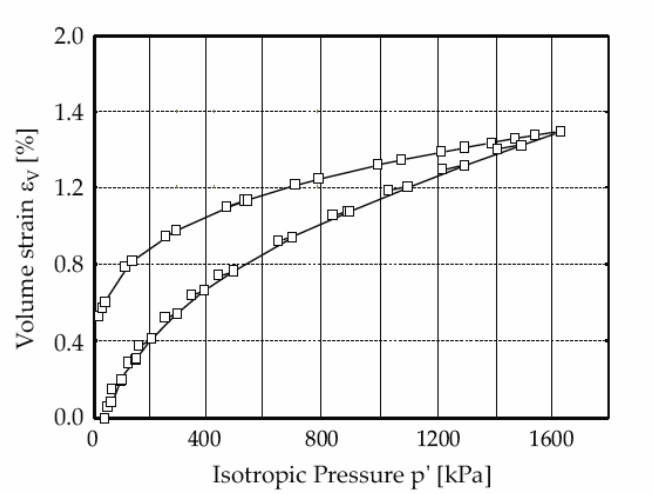

Figure 7. Isotropic compression test interrupted by small-strain cycles (Lade & Abelev, 2005)

Figure 3 illustrates a typical stiffness-strain curve for soil. The figure shows typical ranges of strains for laboratory testing and for structures. At small-strains, the stiffness is relatively large, while at strains close to failure, the stiffness is small. This is soil being non-linear. For small-strain level, G is almost constant. For larger strains which are generally less than a certain limit, the tangent shear modulus G is a non-linear function of strain. In this intermediate small strain range the stiffness decreases smoothly with increasing strain. When the large strain exceeds 1% the stiffness is typically an order of magnitude less than the maximum.

1.3.2 The influence of stress-state

A power law was proposed by (Hardin & Richart, 1963) to determine the relationship between small-strain modulus G_0 and effective mean stress p':

$$G_0 \propto (p')^m$$

(Hardin & Richart, 1963) themselves used the value m = 0.5 for cohesive and non-cohesive soils. Their value for non-cohesive soils is widely confirmed, since all recent studies use the exponent m = 0.40-0.55 (Hoque & Tatsuoka, 2004; Kalliouglou & Papadopoulou, 2003; Kuwano & Jardine, 2002). For cohesive soils no value is adopted yet; many studies confirmed the value m = 0.5 where others found it as high as m = 1.0. Figure 8 and Figure 9 show the variation of m with plasticity index and liquid limit (Viggiani & Atkinson, 1995b) and (Hicher, 1996). By (Viggiani & Atkinson, 1995b), tests were carried out on fine-grained soils (speswhite kaolin clay, powdered slate dust, London clay and North Field clay) in a hydraulic triaxial cell fitted with bender elements. The small-strain shear modulus G_{max} was measured using bender elements. Reconstituted samples were prepared by one-dimensional consolidation of a slurry in a tall floating ring

oedometer until the samples were sufficiently strong to handle. They were then transferred to the hydraulic triaxial cell and consolidated, usually isotropically, to the required initial state. The small-strain shear modulus G_{max} was measured at various states during the test using the bender elements. They interpreted the data by taking the effective length as the distance between the tips of the elements and the arrival of the shear wave as the first significant reversal of polarity of the received signal. The samples were brought to states with p' = 50-400 kPa. The data show that the value of G_{max} increases with mean effective stress p'. Figure 8 shows the variation of the exponent m which relates G_{max} and p' with plasticity index. (Hicher, 1996) used a triaxial apparatus with local deformation transducers in the middle part of the sample in order to measure small deformations. Compression and extension triaxial tests were performed from an isotropic state of stress on various types of clay and compared with results from other authors. Figure 9 shows the influence of liquid limit on the exponent m, which varies between 0.5-0.95. This indicates that when the liquid limit increases, the influence of mean effective stress on small-strain stiffness becomes more important, this is due to increment in compressibility.

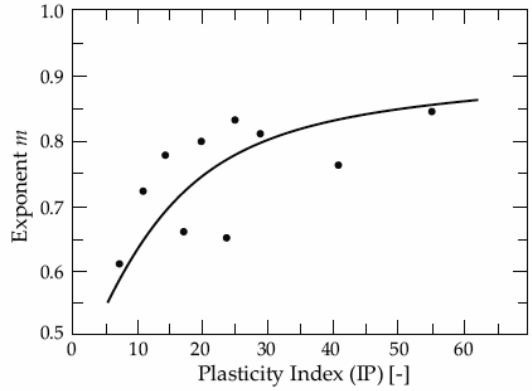

Figure 8. Variation of exponent m with plasticity index after (Viggiani & Atkinson, 1995b).

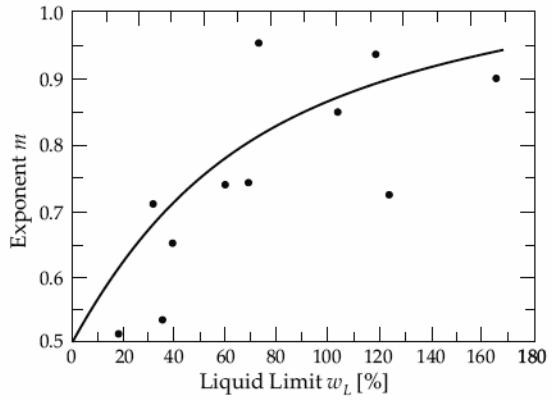

Figure 9. Variation of exponent m with liquid limit (Hicher, 1996).

1.3.3 The influence of soil plasticity

(Vucetic & Dobry, 1991) proposed the shear modulus reduction chart shown in Figure 10. The curves have been compiled from 16 publications (Anderson & Stokoe, 1978; Dobry & Vucetic, 1987; Hardin, 1978; Hardin & Drnevich, 1972; Idriss et al., 1976; Ishihara, 1986; Kim & Novak, 1981; Kokusho et al., 1982; Marcuson & Wahls, 1972; Matsui et al., 1980; Richart, 1975; Richart et al., 1970; Romo & Jaime, 1986; Seed & Idriss, 1970; Vucetic, 1988; Vucetic & Dobry, 1988) and at least 12 research groups. They show the influence of soil plasticity on small-strain stiffness. A large scatter is clear in these curves, therefore, the chart should be used with care especially for PI>30. (Stokoe et al., 2004) measured small- and intermediate-strain stiffness by resonant column and torsional shear tests on samples ranging in PI between 0 and 100. Since $\gamma_{0.7}$ is defined as the shear strain for a stiffness degradation factor of G/G_{max}=0.7, they proposed a linear increase of $\gamma_{0.7}$ from $1*10^{-4}$ for PI=0 up to $6*10^{-4}$ for PI=100.

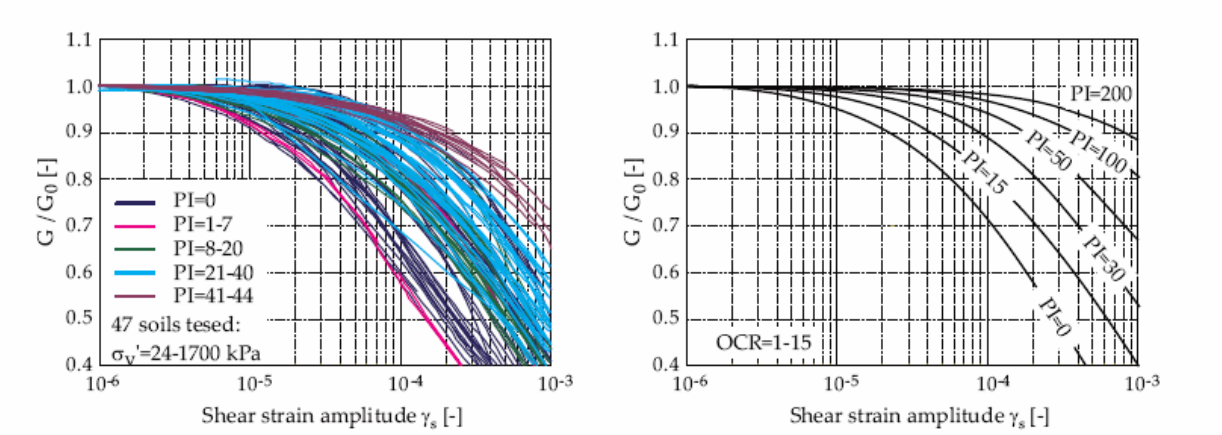

Figure 10. Influence of Plasticity index (PI) on stiffness reduction: Left database for soils with different PI (Hsu & Vucetic, 2002); Right PI chart (Vucetic & Dobry, 1991).

1.3.4 The influence of void ratio

(Hardin & Richart, 1963) measured shear wave velocity on various types of sand using resonant column method. Values of shear wave velocities for various specimens with different void ratios were obtained for various particular values of confining pressure. The velocity was found to vary linearly with void ratio, independent of grain size, gradation, and relative density, i.e. the velocity at 100% relative density may be quite different for two sands; however, their velocity are essentially the same when they are at the same void ratio. Hence, the only effect of grain size and gradation is to change the range of possible void ratios. They proposed a relation between G_0 and void ratio:

$$G_0 \propto \frac{(2.17-e)^2}{1+e}$$ for round-grained sands (e<0.80)

$$G_0 \propto \frac{(2.97-e)^2}{1+e}$$ for angular-grained sands (e>0.60)

Other relationships between G_0 and e found in the literature are typically of the form:

$$G_0 \propto e^{-x}$$

Many researches tried to determine x. (Fioravante, 2000) determined small strain stiffness of two sands with different geological origin via laboratory seismic tests performed in a triaxial cell. Dry triaxial reconstituted specimens of Ticino river silica sand and of Kenya carbonatic sand were subjected to isotropic and anisotropic states of effective stress; then both shear and constrained compression waves were propagated in vertical, horizontal and oblique directions by means of five couples of piezoelectric transducers especially arranged in the specimens. The propagated shear waves allow the assessment of the shear G_0. He found that x=0.8 for sand. (Lo Presti et al., 1993) studied the shear modulus of freshly deposited specimens of two different sands. This modulus was measured in a resonant column and torsional shear apparatus. The soil specimens studied included a calcareous, crushable, well-graded, coarse-to-medium sand containing about 2% fines and a silica, uniform, coarse-to-medium sand without fines (Ticino sand). They found x=1.3 for cemented sand and fine-grained soils. While (Biarez & Hicher, 1994) found x=1 for sand and clay. (Lo Presti & Jamiolkowski, 1998) proposed the range 1.1 – 1.5 for x for various clays. They performed monotonic torsional shear test, resonant column test, compression triaxial test and bender elements in an oedometer apparatus or a triaxial apparatus. The tested material was six different Italian clays with different void ratios.

1.3.5 The influence of overconsolidation ratio (OCR)

The overconsolidation ratio (OCR) is the ratio of maximum past vertical effective stress to the current vertical effective stress. In cohesive soils G_0 increases with overconsolidation ratio. (Hardin & Black, 1968) proposed the following empirical relationship:

$$G_0 \propto OCR^k$$

Where k is a parameter which varies between 0 for sands and 0.5 for high plasticity clays. Later (Hardin & Black, 1968) proposed again another relationship:

$$G_0 \propto R_0^k$$

Where R_0 is the ratio of maximum past effective mean stress to the current effective mean stress. By (Viggiani & Atkinson, 1995b), tests were carried out on fine-grained soils (speswhite kaolin clay, powdered slate dust, London clay and North Field clay) in a hydraulic triaxial cell fitted with bender elements. The small-strain shear modulus was measured using bender elements. The samples were brought to states with p' = 50-400 kPa and R_0 = l-8. They found that the value of G_0 at a particular stress increases with overconsolidation ratio. The data are plotted as (G_0/G_{0nc}) where G_{0nc} is the value of G_0 corresponding to normally consolidated samples at the same mean effective stress (Figure 11). They found that *k* varies between 0.2 and 0.25 for PI=10-40. Since this variation is relatively small from practical point of view, some researches proposed to neglect the influence of OCR on G_0 completely. For non-plastic soils, OCR has a small influence on the small-strain reduction curve.

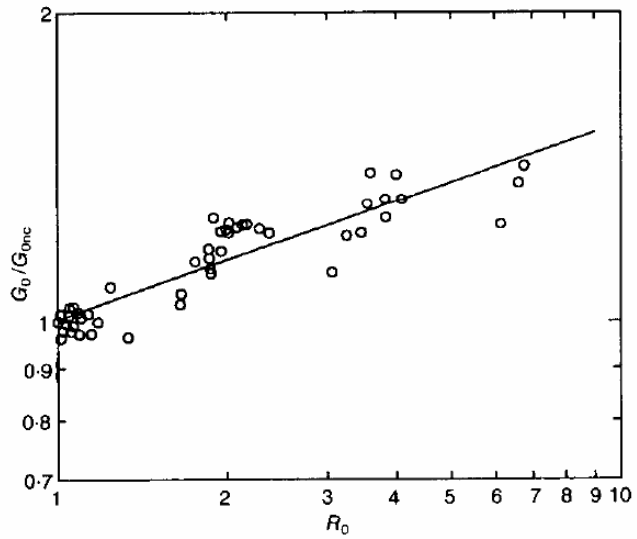

Figure 11. Variation of G_0 with overconsolidation for reconstituted samples of speswhite kaolin

1.3.6 The influence of diagenesis

Diagenesis refers to changing in particle texture, conversion of minerals from one type to another, and formation of interparticle bonds as a result of increased temperature, pressure, and time (Mitchell & Soga, 2005). Diagenetic process alters the stiffness of soils with time. The most important effects of diagenesis are cementation and aging, which are defined as a change in various mechanical properties resulting from secondary compression under a constant external load. Generally, aging is linked to clays, but it can occur in sands, sand stones, and clayey sand. Cementation is caused by natural or artificial soil stabilization processes. Cementation is particularly important for sands. The strength of cemented sand depends on the strength of the cemented agent and the strength

of the sand grains. The evolution of shear wave velocity with cementation is demonstrated using a sand-cement mixture tested in resonant column. Two specimens are isotropically confined to different stresses and allowed to harden at constant confinement: specimen A at σ' = 70 kPa and specimen B at σ' = 415 kPa. Results are shown in Figure 12. The shear wave velocity increases with time. Both specimens asymptotically approach the same stiffness; therefore, cementation prevails over effective stress (Fernandez & Santamarina, 2001). They found that small-strain stiffness of sands can increase by an order of magnitude or more due to cementation.

The term "aging" describes a change of the mechanical properties of a soil with time *t* under constant external stress. Aging effects may cause cementation of the grain contacts or an improvement of their micro- or macro-interlocking due to very small relative movements. (Shibuya et al., 1995) proposed the following equation to estimate the time-dependent increase of G_0 due to aging:

$$\frac{G_0(t)}{G_0(t_p)} = \left[\frac{t}{t_p}\right]^{N_G}$$

where t_p is the time required to reach the end of primary consolidation; *t* is any time ($t > t_p$), $G_0(t_p)$ is the maximum stiffness at time t_p, and N_G is an empirical material factor.

The behavior of naturally or artificially cemented sands is affected by cement content. (Fernandez & Santamarina, 2001) reviewed published experimental studies and presented a microscale analysis is of the effect of cementation on small-strain stiffness. They found that the small-strain stiffness of sands can increase by an order of magnitude or more due to cementation.

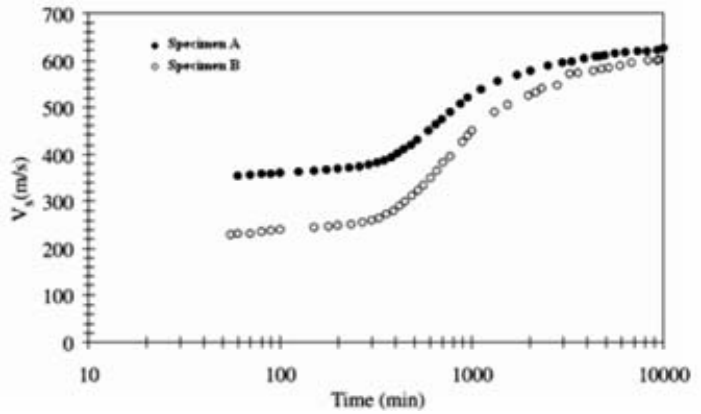

Figure 12. Effect of cementation on shear wave velocity (Fernandez & Santamarina, 2001).

1.3.7 Influence of strain rate

Experimental investigations show that G_0 increases with load rate (e.g. Vucetic & Tabata, 2003). In cohesive soils, the effect of strain rate increases with plasticity index. (Yong & Japp, 1967) defined the strain rate shear modulus parameter as:

$$\alpha G = \frac{\Delta G_S}{\Delta \log \dot{\gamma}}$$

As shown in Figure 13, the strain shear modulus parameter αG defines the slope of the stress versus strain rate line in a semi-logarithmic format. The figure indicates that the strain rate effect increases with strain rate and soil plasticity, but decreases with shear strain amplitude.

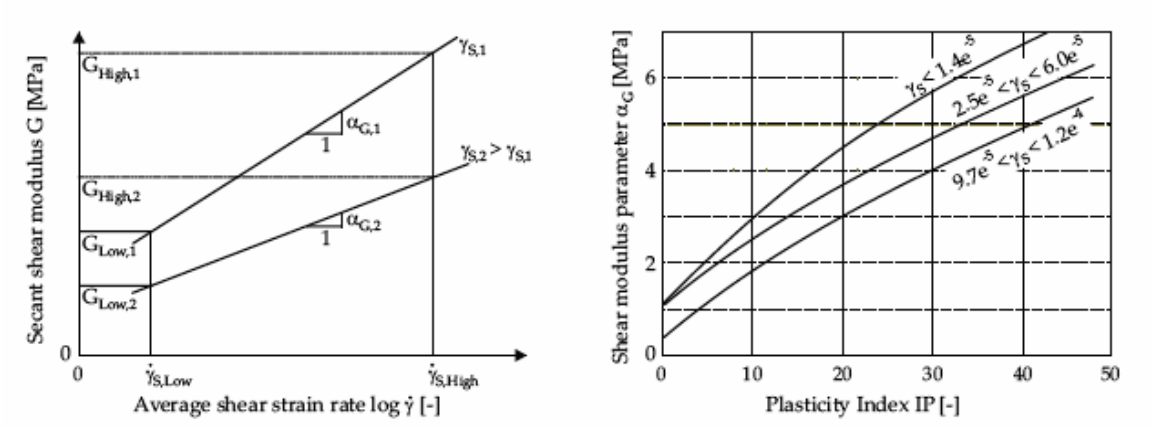

Figure 13. The strain rate shear modulus parameter dependency on strain amplitude and plasticity index (Vucetic et al., 2003)

Figure 13 and Figure 14 show that small-strain stiffness is only a little biased by common straining rates. This is in agreement with the findings of (Stokoe et al., 1999) "For excitation frequencies changing from 1 to about 100 Hz, G_0 increases by about 5% to 30%, with the effect generally increasing with increasing PI". In sands, only a very small or no increase is found (Hicher, 1996). The shear modulus $G_{\max}$ can be obtained from $E_{\max}$ modulus by assuming a value for Poisson's ratio (e.g. Atkinson, 2000), since it is a common simplification to assume that Poisson' ration is constant in the small-strain level, although it increases slightly with applied strain.

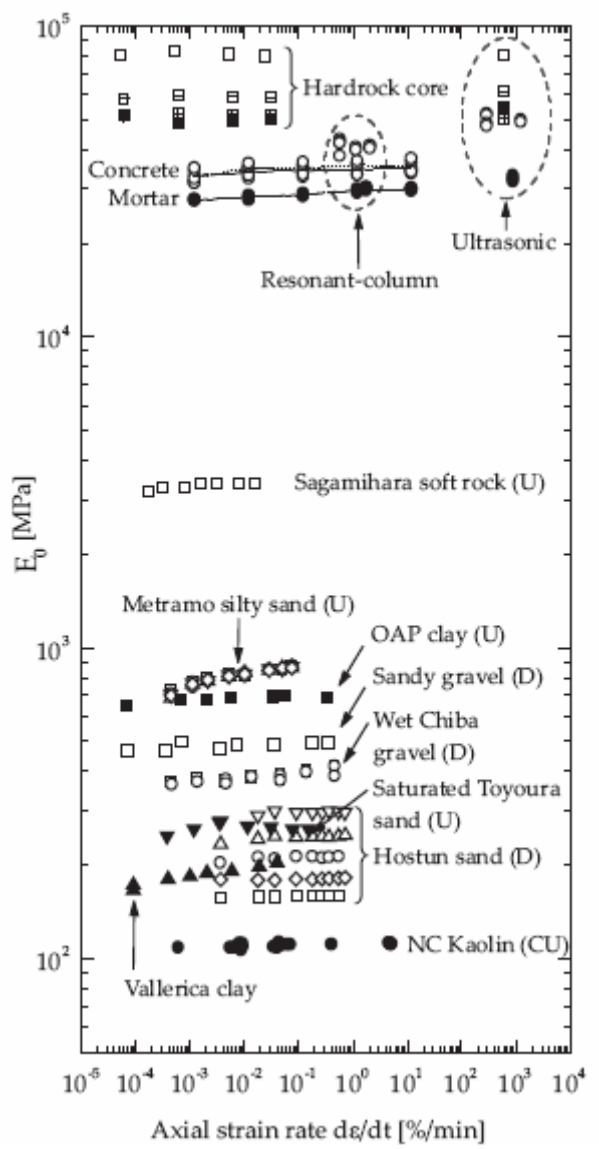

Figure 14. Strain rate effect on the Young´s modulus E_0 (Tatsuoka, 2000).

1.3.8 Other effects that influence small-strain stiffness

The effective friction angle has a small influence on small-strain stiffness (Seed & Idriss, 1970). (Hardin & Richart, 1963) used resonant column method to evaluate shear wave velocity for different sands. They compared shear wave velocities for round grained sand and extremely angular sand. They found that at low confining pressures and comparable void ratios, the shear wave velocity is higher in angular grained sands than in round grained sands. As the confining pressure increases, the velocities in the two materials approach each other. Dilatancy is not activated in the range of such small-strain.

Mean grain diameter and grain size distribution have an influence on small-strain stiffness. (Iwasaki & Tatsouka, 1977) reported a reduction in G_0 about 10-25% in well graded sands compared to poorly graded sands. The addition of 2-5% fines then showed another decrease in G_0 of about 20%.

Capillary increases G_0 with decreasing saturation and decreasing grain diameter, therefore, in partially saturated samples, capillary should be considered in the presence of fines (Stokoe & Santamarina, 2000). With decreasing saturation, fine clay particles increasingly migrate to interparticle contacts of sand and silt grains and they form buttresses and bridges that increase the small-strain stiffness.

1.4 Summary

The influence of various parameters on small-strain stiffness is reviewed. Strain amplitude, void ratio and stress state seem to be the most important parameters that affect the small-strain stiffness of the soil.

Table 1 shows a list of parameters that were discussed in the previous sections with different levels of importance. The table was originally given by (Hardin & Drnevich, 1972) and updated by (Benz, 2007). As it is shown in this table, the most important parameters for small-strain stiffness are strain amplitude, confining pressure, void ratio and diagenesis for clean sands and cohesive soils, and plasticity index and degree of saturation for cohesive soils.

Table 1. Parameters affecting the small-strain stiffness of soils (Benz, 2007), modified from original table presented in (Hardin & Drnevich,1972).

Parameter	Importance to [a]	
	Clean sands	Cohesive soils
Strain amplitude	V	V
Confining Pressure	V	V
Void ratio	V	V
Plasticity index (PI)	-	V
Overconsolidation ratio	R	L
Diagenesis	V	V
Strain rate	R	R
Effective material strength	L	L
Grain characteristics	L	L
Degree of saturation	R	V
Dilatancy	R	R

a. V means very important, L means less important, and R means relative important

Chapter II
Determination of G_{max}

In this chapter, an overview of the most common in-situ and laboratory tests to determine the small-strain stiffness of soil is given. Each test is explained with giving the advantages and disadvantages. In low strain tests, deformations can be assumed as elastic.

2.1 In-Situ Tests

The objective of the in-situ tests is generally to determine the P-wave and/or S-wave velocity in the field. There are two categories of in-situ seismic tests depending on the strain range; small-strain tests and large-strain tests. The second category contains dilatometer test, pressuremeter test, cone penetration test (CPT) and standard penetration test (SPT) etc. These tests provide soil stiffness parameters in the large-strain range. Only the small-strain tests will be discussed in this chapter.

2.1.1 Seismic reflection tests

The seismic reflection test determines the P- and S-wave velocity and superficial layers thickness using the principle of echo-sounding and radar. (ASTM D7128–05) is a code summarizes the technique, equipment, field procedures, data processing, and interpretation methods for the assessment of shallow subsurface conditions using the seismic-reflection test. The test is performed by producing an impulsive disturbance at the source S and measuring the arrival time at the receiver R as shown in Figure 15.

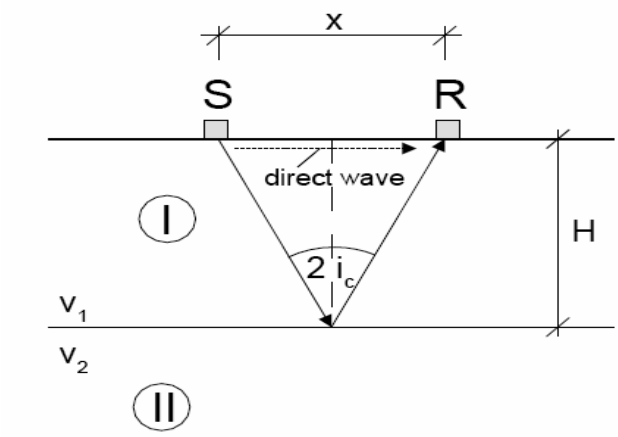

Figure 15. Wave paths in the seismic reflection test (Karl, 2005).

Some of the wave energy follows a direct path from S to R. Another portion of the impulse energy travels downward and strikes the layer boundary. A part of that wave which is reflected back toward the ground surface arrives at the receiver, so the direct

wave and the reflected wave can overlap, therefore it is difficult to determine the arrival time of the reflected wave, particularly of cases in which reflected waves arrive while the receiver is still responding to direct waves. Therefore the difference between the two arrivals should be sufficient, thus, layer should be thick. Furthermore, Arrival times from waves reflected at several layer interfaces have to be distinguishable. Field methods for the acquisition of seismic reflection test vary considerably, depending on whether the area is land or marine, on the nature of the geologic problem, and on the accessibility of the area (Sheriff & Geldart, 1995).

2.1.2 Seismic refraction test

The seismic refraction test involves the measurement of travel times of P- or S-waves from an impulse source to a linear array of receiver points along the ground surface at different distances from the source. The seismic refraction test avoids the reflection test problems by considering the first wave arrival to the receiver regardless of wave path. The setup of a seismic refraction test can be found in (ASTM D5777) and can be done as shown in
Figure 16.

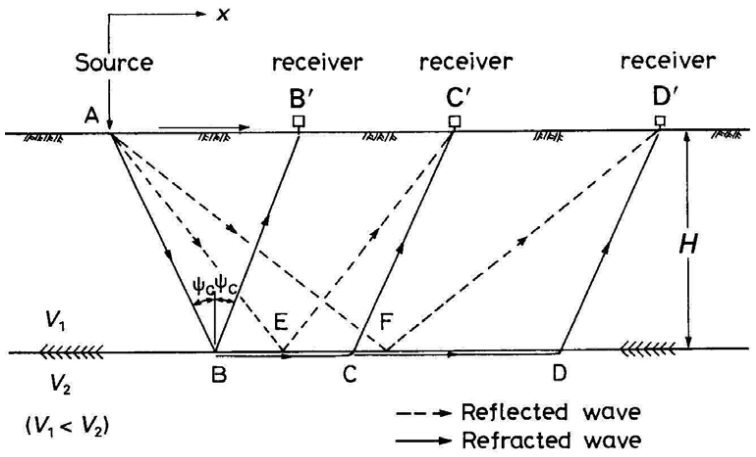

Figure 16. Wave paths in the seismic refraction test (Schmidt, 2000).

The source excitation can be mechanical or explosive. The receivers are usually geo-phones placed in a linear array. One receiver is located at the source. The output of all receivers is recorded when the impulse load is triggered. The method is also applicable for inclined layer interfaces and multi-layered stratifications, if the wave propagation velocity increases with the layer depth. If it is not the case, the results of seismic refraction test can be misleading. A low-velocity layer underlying a higher-velocity layer will not appear as an individual segment on the travel time-distance diagram. Instead, it will cause the computed depths of the layer boundaries to be greater than the actual depths. Details of calculating wave velocities for horizontal layering and inclined or irregular layering can be found in (Kramer, 1996).

2.1.3 Spectral analysis of surface waves (SASW)

The SASW-technique uses the characteristics of Rayleigh waves to obtain the stratification of a site. This method was developed by (Nazarian & Stokoe, 1983; Stokoe et al., 1994). Rayleigh waves travel, as surface waves, in the region close to the soil-air interface. Due to the fact that the penetration depth of the Rayleigh waves into the ground is approximately one wavelength, the thickness of the layer package influencing the speed of the wave changes with the wavelength. This leads to a wave velocity that depends on the wavelength respectively the frequency. Such behavior is also called dispersion.

The SASW test is performed by placing two vertical receivers on the ground surface in line with an impulsive or random noise source, as illustrated in Figure 17. The wave arrival in at least two points at some distance from the source is recorded. The output of both receivers is recorded and transformed to the frequency domain using the fats Fourier transform. After transformation, the phase difference, $\phi(f)$, can be calculated for each frequency. The corresponding travel time between receivers can be calculated for each frequency from:

$$\Delta t(f) = \frac{\phi(f)}{2\pi f}$$

Since the distance between receivers, $\Delta t = d_2 - d_1$, is known, the Rayleigh wave phase velocity and wavelength can be calculated as function of frequency:

$$v_R(f) = \frac{\Delta d}{\Delta t(f)}$$

$$\lambda_R(f) = \frac{v_R(f)}{f}$$

With modern electronic instrumentation, these calculations can be performed in the field virtually in real time. The unwrapped phase of this spectrum is used to calculate an experimental dispersion curve of the Rayleigh wave velocity.

The shear wave velocity and shear damping ratio profiles are determined separately. (Lai et al., 2002) presented a procedure to measure and invert surface wave dispersion and attenuation data simultaneously and, thus, account for the close coupling between the two quantities. The methodology also introduced consistency between phase velocity and attenuation measurements by using the same experimental configuration for both. Characteristic statistics, statistical distribution, and measurement uncertainty were determined for each phase of SASW by (Marosi & Hiltunen, 2004). Using the empirical statistical properties and measurement uncertainty results as validation criteria, an analytically based uncertainty assessment system was developed

SASW test has important advantages over other field tests; they require no boreholes, can be performed quickly, and can detect low velocity layers. SASW testing is particularly useful at sites where drilling and sampling are difficult. On the other hand, this test requires specialized equipments and experienced operator.

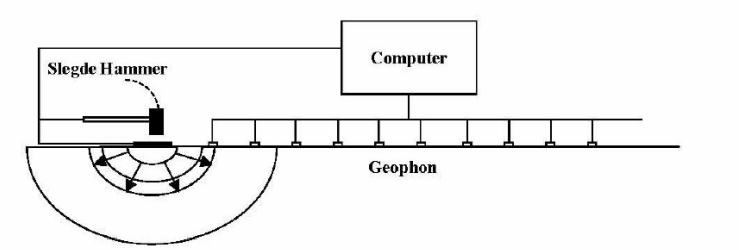

Figure 17. Typical configuration of source and receivers in a SASW test (Schmidt & Schlesinger, 2005).

2.1.4 Seismic cross-hole test

The seismic cross-hole test measures the P- and S-wave velocities between boreholes. The procedures are described in (ASTM D4428). The simplest configuration consists of two boreholes. The first one contains the source which can be mechanical or explosive. In the second one the receiver is installed at the same depth as the source. By testing at various depths, a velocity profile can be obtained. To avoid inaccuracies resulting from trigger time measurements, casing and backfill effect, and site anisotropy, it is preferred to use more than two receivers as in Figure 18. Wave velocity can then be calculated from differences in arrival times. Arrival time can be determined by (first arrival, first peak, first through, etc.) or by cross-correlation technique. In first arrival, travel time is calculated between the start of input signal and the first deflection from zero line in the output signal. Travel time can also be calculated between the first peak in the input signal and the first peak in the output signal for first peak method, and similar for first through method. For the cross-correlation technique, travel time is taken as the time shift that produces the peak cross-correlation between signals recorded. This technique is favorable because first deflection, first peak or first through can be difficult to determine, especially with the existence of noise. Typical distances between the boreholes are 5 to 12 m for layered soils and up to 30 m for nearly homogeneous sites. Cross-hole test can yield reliable velocity data to depths of 30-60 m using mechanical impulse sources, and to greater depths with explosive sources (Kramer, 1996).

Cross-hole tomography test is an extension of the conventional cross-hole seismic test. It uses a string of receivers instead of just one, so that multiple ray paths can be recorded for a single source signal (Pihl et al., 1986). Amplitude attenuation measurements from cross-hole tests involving three or more boreholes has been used to compute the material damping ratio of soils (EPRI, 1993).

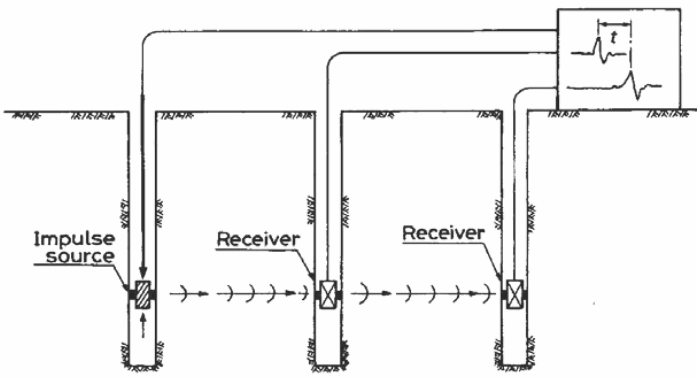

Figure 18. Seismic cross-hole test (Schmidt & Wuttke, 2004).

2.1.5 Seismic down-hole and up-hole test

The down-hole or up-hole test is performed in one borehole. In the down-hole test (Figure 19), the receiver is in the borehole which can be moved to different depths to measure different layers, and the source in located on the surface near the borehole. In the up-hole test, it is vice versa, the source is situated in the borehole, and the receiver is on the surface. ASTM D7400 is the standard test methods for down-hole seismic testing.

Since waves can be more easily generated on the surface than in the borehole, the down-hole test is more practical in use; therefore, it is more commonly used.

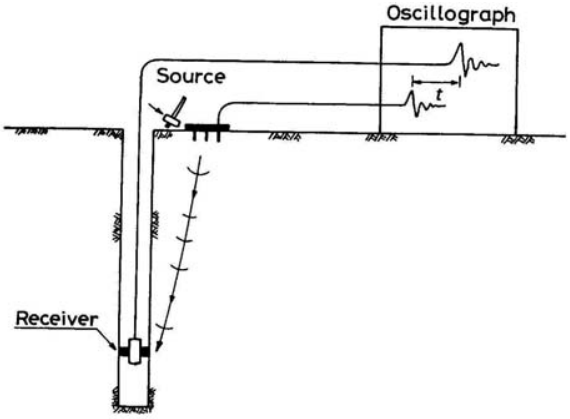

Figure 19. Seismic down-hole test (Schmidt, 2000).

The down-hole test detects layers which can be hidden in the seismic refraction surveys. It also requires only one borehole, which is less costly and complicated than seismic cross-hole test. On the other hand, drilling of the borehole, like other tests which need boreholes, can disturb the soils around it. Also uncertainties can result from background noise effect, groundwater table effects, etc.

2.1.6 Seismic cone penetration test

The seismic cone penetration test (SCPT) (Robertson et al., 1985) can be seen as a special version of a down-hole test with the receivers (geophones or accelerometers) installed in the tip of a cone pushed into the ground by conventional cone penetration equipment, while the source is placed at the surface (Figure 20). An SCPT system includes the following components: (1) an electrical penetrometer, (2) hydraulic pushing system with rods, (3) cable or transmission device, (4) depth recorder, (5) source, and (6) data acquisition unit. The seismic source consists of a steel beam and different types of hammers; a horizontal hammer blow at one end of the beam produces a shear wave dominated pulse and a vertical one blow on top of the beam produces a compression wave dominated pulse. The cone with the receiver is pushed stepwise into the ground. Usual intervals are 0.5 or 1.0 m. At each step the source generates a seismic pulse recorded by the cone receiver. The standard testing method to perform SCPT is ASTM D5778. A variety of cone penetrometer systems is available, ranging from small mini-pushing units to very large truck and track vehicles. The penetrometers are normally available in two standard sizes: (1) a 35.7-mm diameter version having a corresponding cross-sectional area of 10 cm^2; and (2) a 44-mm diameter version. (Kurup, 2006) integrated several sensing techniques with the cone penetrometer technology. These include a camera for visual identification, and various sensors for measuring stresses, pore water pressure, shear wave velocity, electrical conductivity, temperature, oxidation-reduction potential, radioactivity, and hydrocarbon contamination in soils. Since no borehole is necessary the test is much less expensive than a down-hole test.

Figure 20. A modified truck for SCPT test (Karl, 2005).

2.2 Laboratory Tests

A limited number of laboratory tests is performed in the range of small-strain. They include local deformation transducers, resonant column test, piezoelectric bender element test and ultrasonic test.

2.2.1 Local deformation transducers

In triaxial testing device, displacement is usually measured between the top cap and the base pedestal, using a global transducer. The accuracy of such transducer is not enough to measure the small-strain. Furthermore, the sample may have no parallel and smooth ends; therefore, the top cap has probably no perfect full instant contact at the small-strain range. The restraints at the ends of the sample cause non-uniform displacements over the height. Local deformation transducers (LDTs) avoid such problems of imperfect bedding. They are installed typically in a triaxial cell. They can measure deformations axially or radially as shown in Figure 21. Local deformation can measure strain of $5*10^{-5}$. Several transducers may be used simultaneously in order to observe the loss of homogeneity of the strain field in the specimen.

Figure 21. Axial and radial deformation transducers.

Local deformation transducers are convenient up to a specific strain limit, after which they could be destroyed. They can disturb the specimen (especially porous rock) due to the penetration of glue inside the pores. They measure displacements between two specific points to deduce strain in the specimen, assuming that deformations in the specimen are homogeneous.

2.2.2 Resonant column

The resonant column test is a well-known technique to determine the dynamic shear modulus, dynamic elasticity modulus and damping ratio. First proposed in 1930s, and then further developed in 1970s, mainly applied for strain levels of 10^{-4}-10^{-2}%. In a triaxial cell a soil sample is installed and excited torsionally or axially at its top end. The excitation is most commonly harmonic, in a range between 30 and 300 Hz, but also random noise or pulses have been used. There are devices for cylindrical samples and for hollow-cylindrical samples available, the latter minimize the variation of shear strain amplitudes across the sample in the case of torsional excitation. With a built in accelerometer, the acceleration at the top of the sample can be measured.

The principle of a resonant column device is based on a cylinder, which is set into torsional or axially vibration. The excitation is most commonly harmonic, in a range between 30 and 300 Hz. The frequency increases until resonance occurs. Under the assumption of a linear elastic material the shear wave velocity is determined from the wavelength and the resonance frequency in the fundamental mode of vibration. The fundamental frequency is a function of the small-strain stiffness of the soil, the geometry of the specimen and certain characteristics of the resonant column apparatus. The specimen can be free at each end so that its lowest mode of vibration is with one node located at the center of the specimen. This type is called the free-free type. In which the specimen is excited at the bottom and the response is picked up at the top. In fixed-free type, both driver and pickup are located at the top end of the specimen.

2.2.3 Bender elements

The bender element method is a simple technique to obtain the very small-strain elastic shear modulus of a soil G_{max} by measuring the velocity of propagation of a shear wave through a sample. The concept of bender elements and their advantages and disadvantaged will discussed with details in the following chapters.

2.3 Summary

In this chapter a general outline of the small-strain tests in both in-situ and laboratory was given. The in-situ tests do not show the effects of other conditions than the current in-situ condition. They require specialized costly equipments and experienced operator and sometimes boreholes in addition to complicated data interpretation. Some of these tests are limited. There is a variety of sources of errors (i.e. background noise, groundwater table effects). The laboratory tests give the opportunity to measure the small-strain under different conditions, but unfortunately, there is limited number of such tests with a

number of disadvantages in each. Bender elements may give a good alternative test to measure G_{max}. A comparison between bender elements and resonant column tests are presented in the next chapter.

Chapter III
Wave Propagation

3.1 Wave Propagation

Mechanical waves can be divided into body and surface waves. Body waves can exist in an ideal full space or they travel in a region that is not affected by a free surface. P- (primary, compression, longitudinal) waves and S- (secondary, shear, transverse) waves are types of body waves. The particle motion of P-waves is in propagation direction; the particle motion of S-waves is perpendicular to the direction of propagation (Figure 22). Surface waves may only exist at the surface or the boundary, separating media of different properties. Rayleigh (vertically polarized) and Love (horizontally polarized) waves are examples of surface waves. Since the velocity of P-waves is highly affected by the groundwater table, the most efforts are spent to the determination of the S-wave velocity. S-waves are transmitted in saturated soils by the soil fabric only. The dynamic shear modulus, G_{max}, can be calculated directly based on the S-wave velocity.

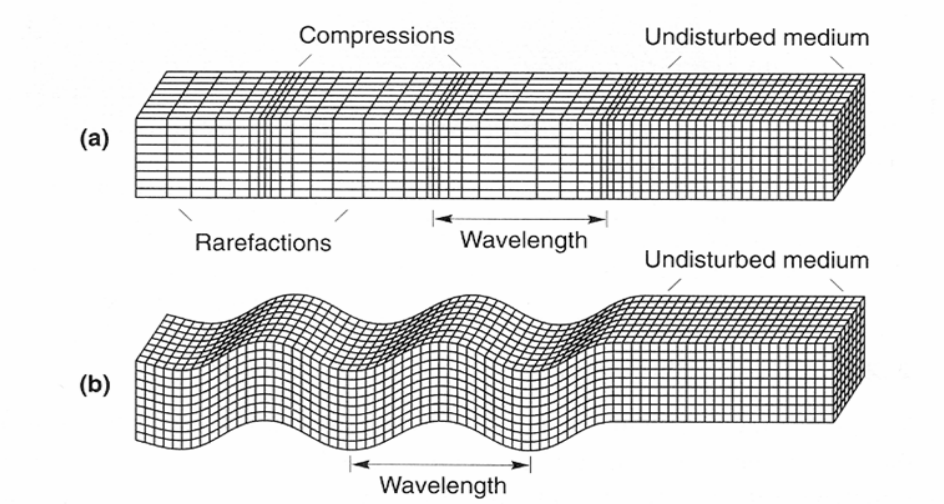

Figure 22. Deformation produced by body waves: (a) P-wave; (b) S-wave (Kramer, 1996).

There are four material parameters which govern wave propagation: bulk stiffness B, shear stiffness G, Mass density ρ and intrinsic attenuation. From the elastic wave propagation theory:

$$G_{max} = \rho \, Vs^2$$

Where G_{max} is in Pa, ρ in Kg/m^3, Vs in m/s.

Table 2 presents typical wave velocity and densities for various materials. One can notice that P-waves velocity for granular material at low confining pressure can be lower than P-waves velocity for air.

3.1.1 P-wave

In a saturated soil, P-waves velocity is affected primarily by the fluid bulk modulus Bf, and less affected also by grain bulk modulus *Bg* and porosity n (Ishihara et al., 1998). Figure 23 presents the effect of porosity on P-wave velocity in a saturated soil. With higher porosity the ratio *Vp*-soil/*Vp-f* decreases, where *Vp*-soil is the P-wave velocity in soil and *Vp*-f is the P-wave velocity in pure water which is 1480m/s. Figure 24 explains the interrelationship between *Vp*, degree of saturation S_r, and Skempten´s parameter (Ishihara et al. 1998).

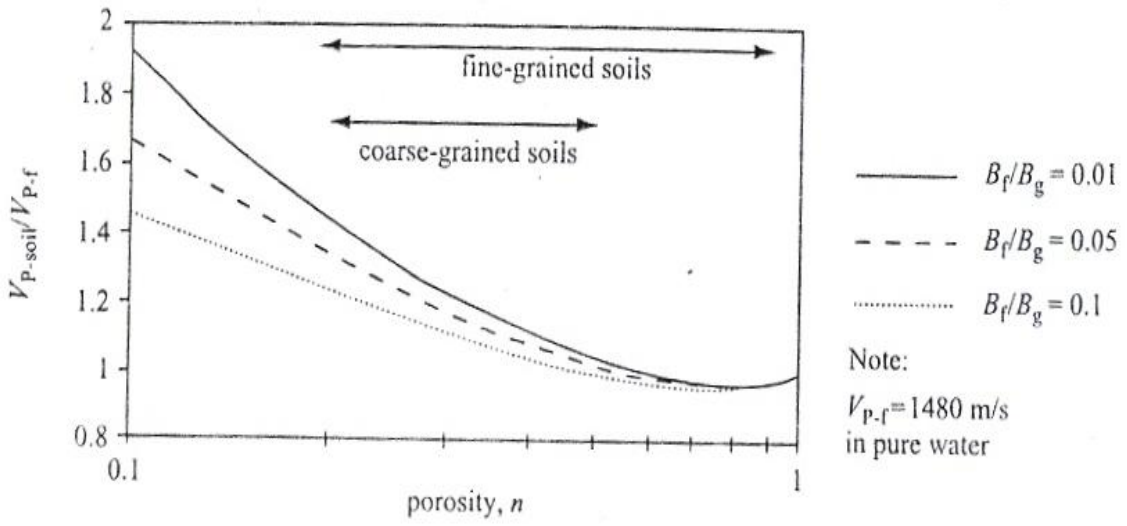

Figure 23. Effect of porosity n on P-wave velocity in a saturated soil (Ishihara et al., 1998).

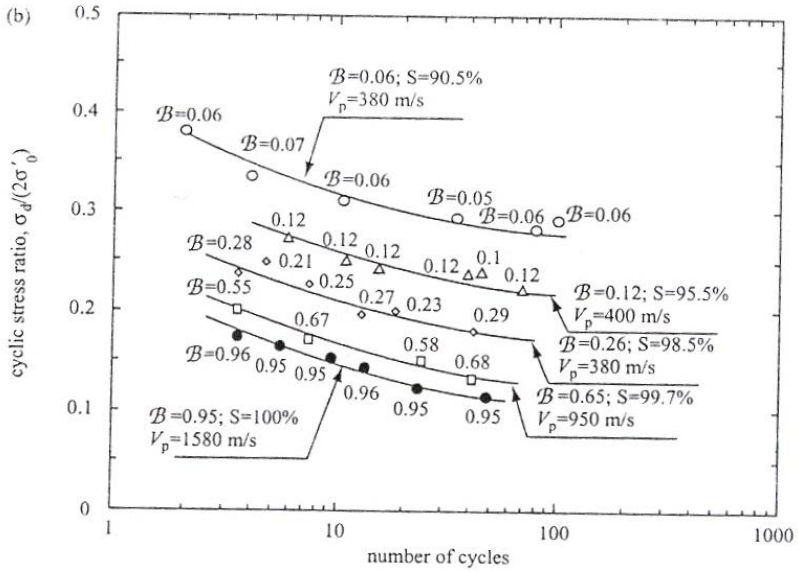

Figure 24. The interrelationship between *Vp*, degree of saturation S_r, and Skempten´s parameter (Ishihara et al. 1998).

Table 2. Typical wave velocity for various materials (Carmichael, 1982, 1989); (Weast, 1988); (Guéguen and Palciauskas 1994).

Wave velocity and density (typical values)

	V_p (m/s)	Density ρ (kg/m^3)
Fluids		
Air (20° C, 1 atm)	0% RH: 343 100% RH: 345	1.204
Pure water	1480	998
Seawater	1531	1025
Benzene	1320	899
Castor oil	1540	969
Glycerin	1920	1260
Minerals		
Salt	4600	2160
K – Feldspar	5600	2560
Quartz	6100	2650
Calcite	6600	2710
Dolomite	7400	2870
Pyrite	8400	5020
Rocks		
Limestone	4000 – 7000	2200 – 2750
Sandstone	2000 – 5500	1950 – 2600
Anhydrite	5600	3000
Granite	5200	2690
Basalt	5900	2850
Shale	2200	1900
Soils (at 100 kPa confinement)		
Granular salt (dry)	230	1300 – 1500
Sand (dry)	120 – 170	1500 – 1900
Clay (saturated)	V_S = 60 – 150	1800 – 2200
Other materials		
Ice	3000 – 4000	917
Wood	4100	800
Plexiglass	2700	1200
Teflon	1400	2200
Metals		
Aluminum	6400	2700
Copper	5000	8930
Steel	5900	7900
Lead	1900	11400
Nickel	5500	8850

Note: S-wave velocity in solids can be computed from P-wave velocity. For $\nu = 0.1$, $V_S = 0.67\ V_P$; for $\nu = 0.25$, $V_S = 0.58\ V_P$.

3.1.2 S-wave

The S-wave velocity is controlled by the skeleton stiffness and density of the soil which depends on the degree of saturation.

With increasing the degree of saturation the skeleton stiffness decreases, therefore the shear wave velocity also decreases (Figure 25). The ratio between shear wave velocity for a dry granular material and shear wave velocity for a saturated same material may vary (2-20) times (Cho & Santamarina, 2001).

Equilibrium analysis in saturated media leads to Terzaghi's effective stress:

$$\sigma' = \sigma - u_w$$

Likewise, the negative pore-water pressure that develops in an unsaturated medium affects the effective interparticle forces. However, the equilibrium analysis must take into consideration the reduced area occupied by the water in the pores. (Bishop,1959; Bishop, 1961) proposed a modified expression for the effective stress in an unsaturated soil:

$$\sigma' = (\sigma - u_a) + \chi(u_a - u_w)$$

where χ = parameter to be experimentally determined. To a first approximation, the parameter χ varies with the degree of saturation, from $\chi = 1$ for saturated soils, to $\chi = 0$ for dry soils. However, χ also depends on wetting history, loading path, soil type and internal structure of the soil. Still, the inadequacy in Bishop's equation goes beyond the difficulty in predicting the value of χ, and it can fail to explain phenomena such as the collapse of some soils upon wetting (u_w decrease σ' decreases, yet massive volume change takes place). The limitations in Bishop's equation can be discussed from different perspectives. On the one hand, it involves a soil parameter χ as in a constitutive equation rather than being a description of the state of stress. On the other hand, it mixes global and local conditions. Today's macroscale interpretation of unsaturated materials is based on separate state variables, such as (u_a - u_w) and (σ - u_a) to avoid such limitations (Bishop and Blight 1963; Fredlund et al. 1978).

(Qian et al., 1991) used a resonant column device to measure the shear of stiffness of unsaturated soils. They tested soil specimens with different degree of saturation S_r, and external confining pressure σ. They observed that shear stiffness has a peak at a certain degree of saturation and that this peak depends on the confining pressure as shown in Figure 26.

Shear wave causes compression in some regions and dilation in others, therefore shear wave causes fluid flow, while compressional wave do not. In fully saturated media, the attenuation for shear waves is higher than for compression waves. (Winkler and Nur, 1979) found that compression losses in saturated media are less than one-third of the shear losses. In unsaturated media, the gas-water mixture has a high compressibility which enhances fluid flow mechanism in compression mode, therefore compression waves attenuation increases while shear waves attenuation decreases. Thus, energy losses

in the compression mode can be as twice as shear mode losses. (Murphy et al. 1984; Murphy et al., 1986)

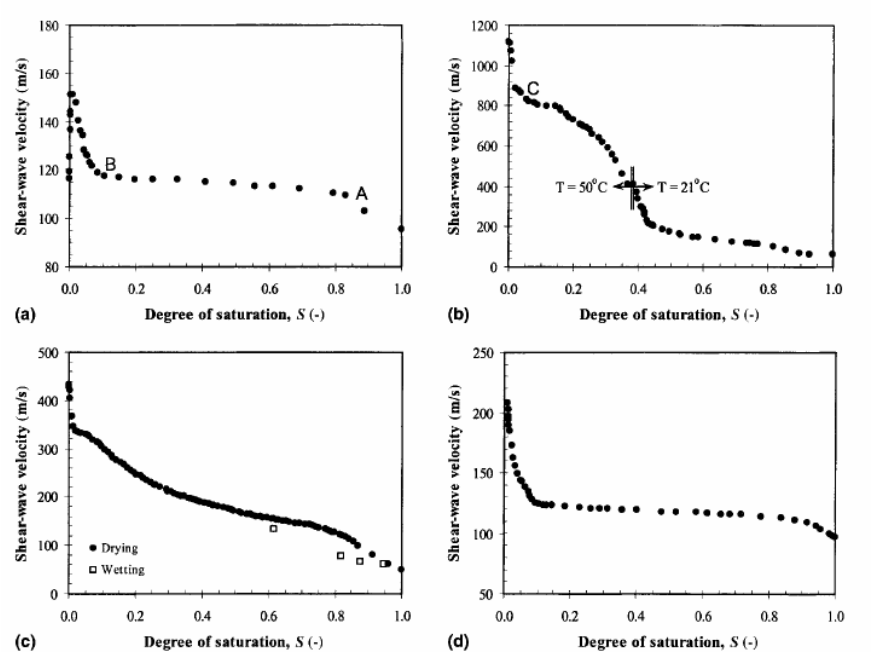

Figure 25. Shear wave velocity versus degree of saturation (a) Clean Glass Beads (Deionized Water); (b) Mixture of Kaolinite and Glass Beads; (c) Granite Powder; (d) Sandboil Sand (Cho & Santamarina, 2001).

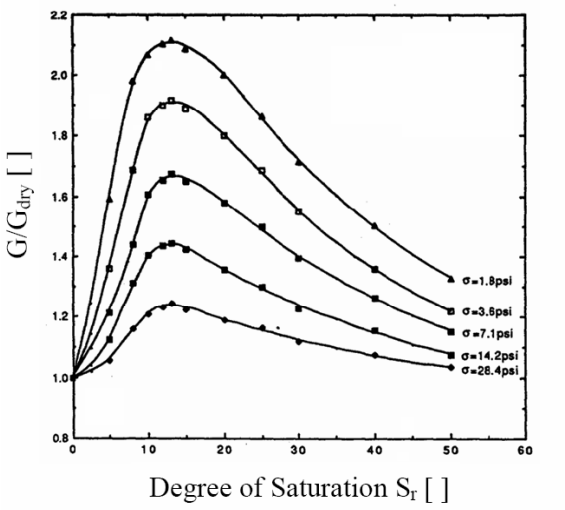

Figure 26. Shear stiffness of unsaturated soils versus degree of saturation and confining pressure (Qian et al., 1991).

Chapter IV
Bender Elements

4.1 History

The history of piezoelectricity dates back to 1880 when Pierre and Jacques Curie first discovered the piezoelectric effect in various substances including Rochelle salt and quartz. Piezoelectric materials can generate an electric charge with the application of pressure; conversely, they can change physical dimensions with the application of an electric field (called *converse piezoelectricity*). The word *Piezoelectricity* comes from Greek; *Piezo* means Pressure in Greek, so the term *(Piezoelectricity)* means (*electricity by pressure*).

In material which has piezoelectric properties, ions can be moved more easily along some crystal axes than others. Pressure in certain directions results in a displacement of ions such that opposite faces of the crystal assume opposite charges. When pressure is released, the ions return to original positions.

The first practical application for piezoelectric devices war sonar, first developed during World War I. The use of piezoelectricity in sonar created intense development interest in piezoelectric devices. Over the next few decades, new piezoelectric materials and new applications for those materials were explored and developed.

4.2 Concept

Piezoelectric materials play an important role in non-destructive testing and in the daily life, from ultrasonic applications in medicine, in optical communications, in military and civilian field to smart sensor systems in cars.

By putting piezoelectric material under mechanical stress, a shifting of the positive and negative charge centers of the elementary units in the material takes place, which then shows up in an external electrical field. This effect is proportional to the deformation, which depends on the state of tension found in the corresponding material. Reversed, an outer electrical field either stretches or compresses such material. A piezoceramic is therefore capable of acting as either a sensing or transmitting element, or both.

Two main groups of materials are used for piezoelectric transducer: piezoelectric ceramics and single crystal materials. The ceramic materials have a piezoelectric constant/sensitivity that is roughly two orders of magnitude higher than those of single crystal materials and can be produced by inexpensive sintering processes. Unfortunately their high sensitivity degrades over time. The less sensitive crystal materials (gallium phosphate, quartz, and tourmaline) have a much higher – when carefully handled, almost infinite – long term stability.

The crystal cell should have no center of symmetry. Just 21 types of total 32 crystal types show this property, therefore, there are many different piezoelectric materials (Krautkrämer & Krautkrämer, 1990). Figure 27 shows the centro-symmetric cubic (isotropic) before poling and after poling exhibit tetragonal symmetry (anisotropic

structure) below the Curie temperature, at which the crystal structure changes from a non-symmetrical (piezoelectric) to a symmetrical (non-piezoelectric) form.

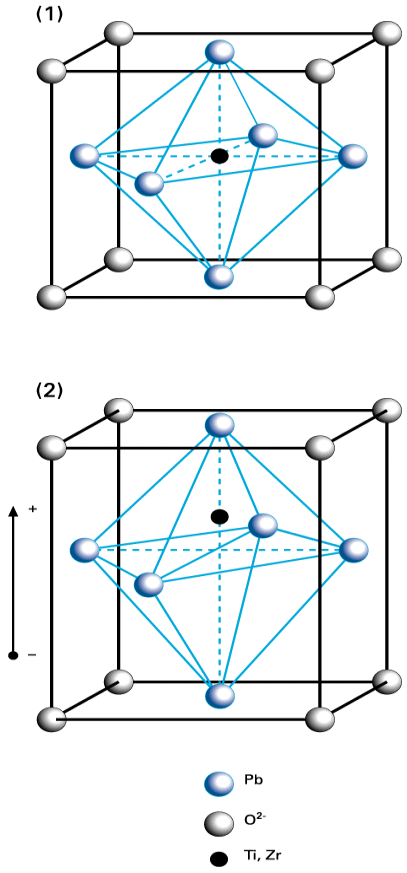

Figure 27. Structure of piezoelectric material.

4.3 Types

There two types of electric operation are used to connect piezo layers; *series connection and parallel connection,* (Figure 28). Series connection refers to the case where supply voltage is applied across all piezo layers at once. The voltage on any individual layer is the supply voltage divided by the total number of layers. A 2-layer device wired for series operation uses only two wires (one attached to each outside electrode). Parallel connection refers to the case where the supply voltage is applied to each layer individually. This means accessing and attaching wires to each layer. A 2-layer bending element wired for parallel operation requires three wires (one attached to each outside electrode and one attached to the center shim). For the same motion, a 2-layer element poled for parallel connection needs only half the voltage required for series connection, therefore parallel-connection-elements are preferred as actuators while series-connection-

elements are preferred as sensors.

Figure 29 and Figure 30 show different types of piezoelectric actuators (motors) and sensors (generators) with some simple linear equations which indicate the relationship among voltage, displacement and dimension of the actuator or sensor. Where Q is the charge, F is the force, V is the voltage, d_{31} and g_{31} are factors, W is the element width and L is the element length.

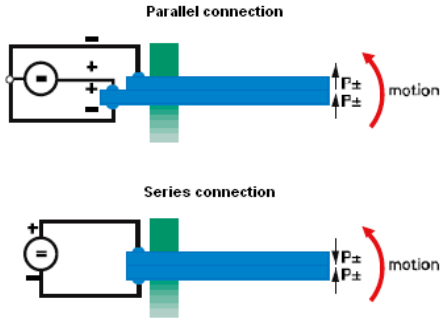

Figure 28. Series connection and parallel connection.

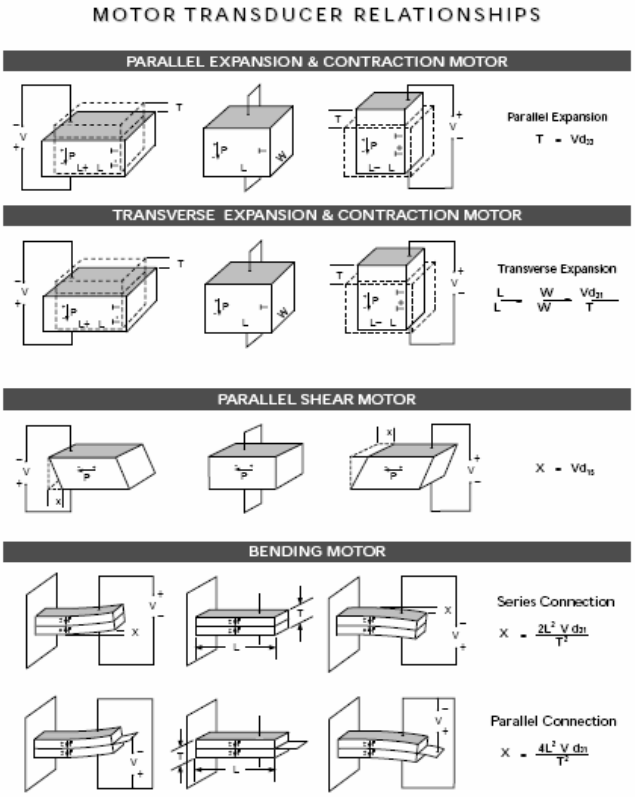

Figure 29. Simple linear equations for piezo actuators (motors).

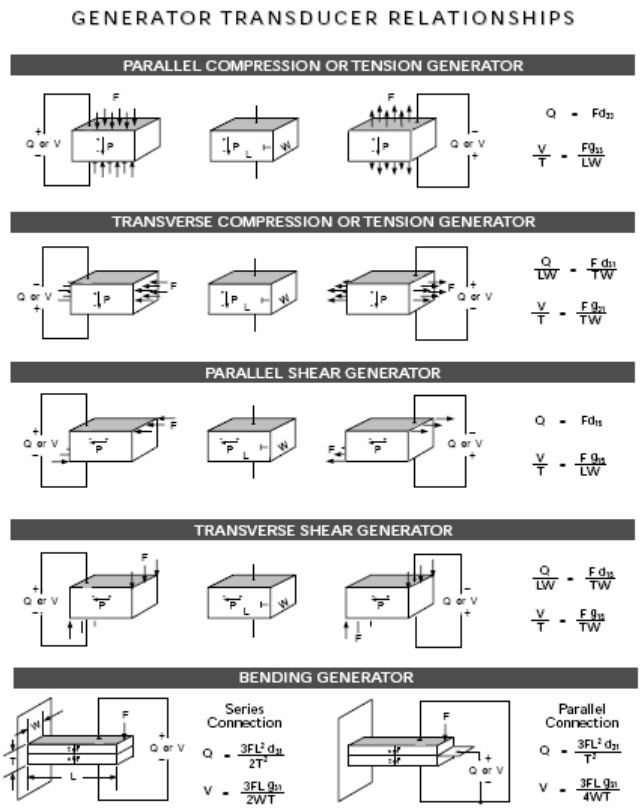

Figure 30. Simple linear equations for piezo sensors (generators).

4.4 Technical Properties

Relationships between applied forces and the resultant responses depend upon: the piezoelectric properties of the ceramic; the size and shape of the piece; and the direction of the electrical and mechanical excitation. There are some piezoelectric coefficients which determine the response of the bender elements. Some of these coefficients specify either a mechanical or electrical properties. The constants *d*, *g*, Young's modulus and Electromechanical coupling coefficient *k* determine the exchange from electrical energy to mechanical one and vice versa. This is important to determine the response of the piezoelectric element especially the maximum amplitude.

"*d*" Constant:
This constant relates the mechanical strain produced by an applied electric field (Figure 31). The units may then be expressed as meters per meter, per volts per meter

$$d = \frac{\text{strain development}}{\text{applied electric field}}$$

d relates to strain for a given electric field which is usually sought in transmitters.

"*g*" Constant

"*g*" is the ratio of strain developed over the applied charge density with units of meters per meter over coulombs per square meter

$$g = \frac{\text{strain developed}}{\text{applied charge density}}$$

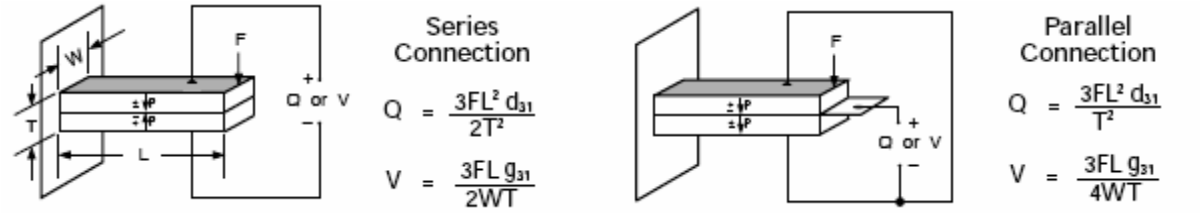

Figure 31. Relationships between applied forces and the resultant responses (Piezo systems Inc.)

There are many other electrical and mechanical properties and factors like Electromechanical coupling coefficient *k*, Dielectric constant *K*, Curie Temperature, Young's modulus, Frequency constant *N*, Mechanical *Qm*, Dielectric dissipation factor, aging rate (Lionetto et al., 2004). Most of them play no role in the field of geotechnics, but some of them have influence on the results in non-destructive test for soil.

4.5 Advantages & Disadvantages

An advantage of this method is that the computation of G_{max} is more direct and simple than other methods like the resonant column test or in-situ tests. Bender elements are easy to install into most soil testing apparatus (i.e., triaxial test, shear test, resonant column test and oedometer test) (Figure 32). The bender elements themselves are cheap, small and lightweight, furthermore they are non-destructive.

Figure 32. Bender elements installed in top cap and pedestal of a triaxial cell.

Regarding the disadvantages, this method is based on the idea of one-dimensional wave propagation, therefore a plane wave is assumed to be propagated in the medium. In reality, the case is three-dimensional wave propagation from a not-perfect-point source causing the near-field effect. Furthermore, the specimen has its boundaries; therefore, there is reflection and interference of waves. Another hypothetical assumption is considering the material isotropic, uniform and continuum, which disregards travel path and dispersion. Sufficient contact should be between the bender elements and the surrounding soil in order to transmit the mechanical wave from the elements to the soil. If this was not the case, the received signal can be unclear and difficult to be analyzed, especially for soils with large particles. That is why it is better to have minimum penetration in the soil according to the particles diameter.

4.6 Effects to Bender Elements

(Shirley and Hampton, 1978) first developed bender elements transducers to measure shear-waves in laboratory, using two ceramic piezoelectric elements fixed diametrically in a cylindrical aluminium pot. The dimensions of the bender elements were 1.27 cm in both thickness and width and 2.54 cm in length, this very large thickness allows only a very small displacement ($5.6*10^{-7}$ m). The receiver was fixed, whereas the transmitter was radially movable in and out of the cylindrical pot in order to measure shear wave velocities for different transmitter-receiver distances. This technique was not successful since these velocities were different due to soil compression and disturbance by transmitter movement.

(Shirley, 1978) achieved farther improvement using a transducer includes two different elements: a bender element which produces shear waves; and a compressional wave element. The bender elements transducer incorporates a small compressional wave element to facilitate the measurements of both shear wave and compressional wave over the same propagation path. The compressional wave element consists of a thin piezoelectric ceramic plate which is polarized and driven in its thinnest dimension.

4.6.1 Technical properties

In general, larger the penetration, the voltage signal is clearer but at the same time, it creates larger disturbance to the sample. On the other hand, smaller penetration is better in the sense that they do not cause much disturbance but generated energy may not be sufficient to propagate to the other end of sample or for receiving.

Figure 33 shows the effect of bender elements length on the G_{max} vs. e relationship for isotropically consolidated specimens at 200 kPa. There is no clear influence of the bender elements length on the data results, thus, there is no need to increase this length since it causes further disturbance in the sample and reduces travel path between bender elements causing larger errors in estimating shear wave velocity (TC-29 Report, 2007).

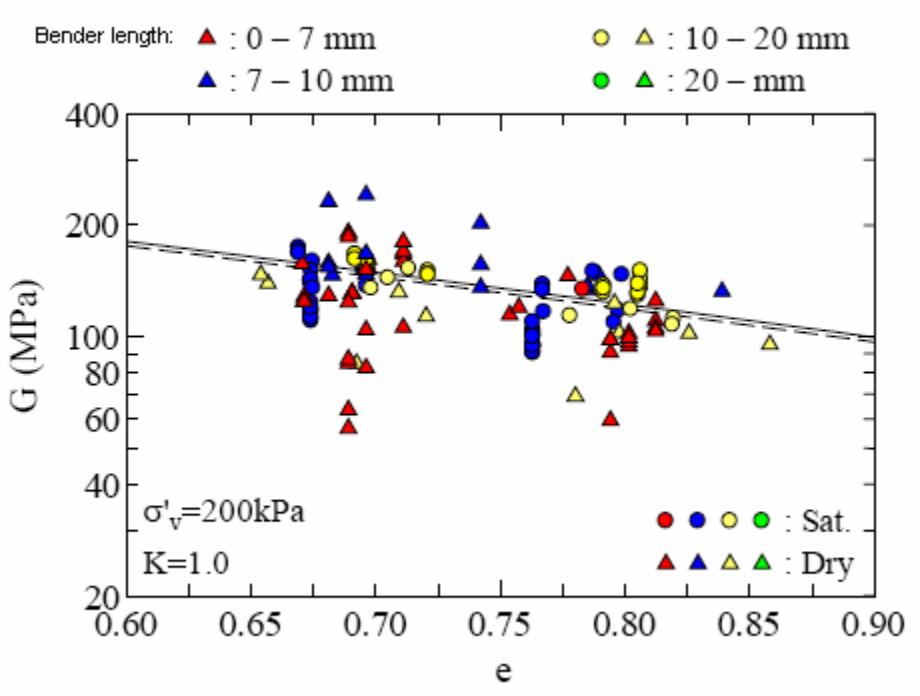

Figure 33. Effects of cantilever length (TC-29 Report, 2007).

(Schultheiss, 1981) recommended using bender elements with an empty cell to make sure that the shear wave is not transferred through the cell frame. He found that effective stress can change bender elements characteristics like resonant frequency.

In its international parallel test on the measurement of G_{max} using bender elements by evaluating the bender element test results from 23 institutions from 11 countries, Technical committee, TC29 (Stress-strain and Strength Testing of Geomaterials) of International Society of Soil Mechanics and Geotechnical Engineering (ISSMGE) did not find any clear influence of the difference in bender size, its structure, cantilever length and wiring method was recognized (TC-29 Report, 2007).

4.6.2 Effective length of samples

Before starting to go into discussion of determining travel time one should determine the sample length as it is a main parameter to calculate velocity. (Viggiani and Atkinson, 1995) did a series of tests of different lengths and different pressures. Figure 34 show travel time against sample length. The three lines are straight and have intercept of about 6 mm on the vertical axis which corresponds with the length of both bender elements (each is 3 mm). Therefore, effective distance should be defined as the distance between the tips of the elements, so-called tip-to-tip. This is in agreement with previous experimental work (e.g. Dyvik & Madshus, 1985).

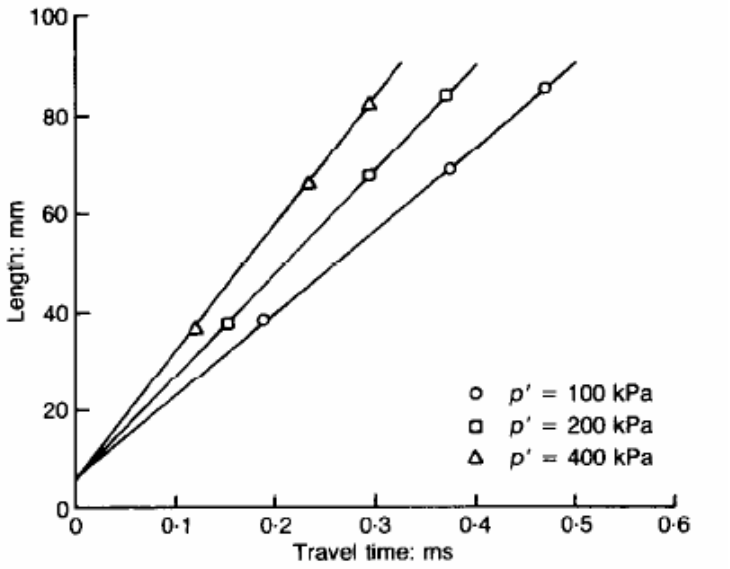

Figure 34. Travel time vs. sample length (Viggiani and Atkinson, 1995).

4.6.3 Near-field evidences

This near-field effect was theoretically analyzed by (Sanchez-Salinero et at., 1986). They showed in their theoretical study that the first deflection of signal may not correspond to the first arrival of the shear wave but to the near-field component. In the near-field, there is a strong coupling between P- and S-wave components. (Sanchez-Salinero et at., 1986) showed the presence of a highly attenuation wave component in the near-field which propagate at P-wave velocity yet with transverse particle motion. That means, the received signal may correspond to shear movement propagates at P-wave velocity, i.e. near-field effect may obscure the S-wave arrival and mask it. This effect becomes significant especially at closer distances between sources and receivers. They developed an analytical solution for the time record at a monitoring point that would result from excitation with a transverse sine pulse of a point source within an infinite isotropic elastic medium. The resulting wave was far from being a simple transversely polarized shear wave propagating in a longitudinal direction. They suggested a criterion, to avoid such an effect. The criterion is regulated by the ratio between the measurement distance, d, and the wavelength λ. Yet, this criterion is not easy to follow due to the dimensional limitations of the testing device

They showed in Figure 35 analytical solution of the motion expressed in term of R_d which is ratio between distance traveled and wave length. Comparison between two signals with two different wave lengths with indicates that signals with low R_d value tend to arrive earlier than the ones with higher values of R_d.

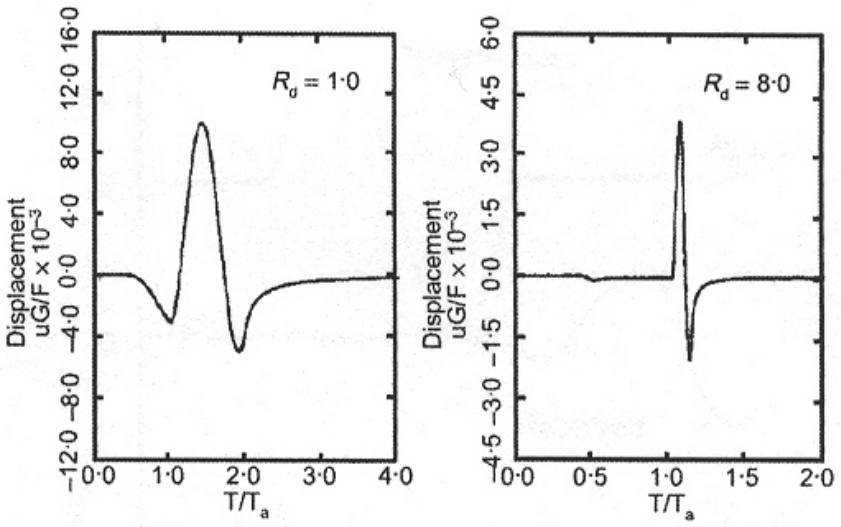

Figure 35. R_d is ratio between distance traveled and wave length; u is particle displacement, and F is amplitude of loading force (Sanches-Salinero et al., 1986).

(Jovičić et al., 1996) proved the effect of the near-field. Figure 36 shows two traces with different R_d values of 1.1 and 8.1, which correspond in this case to frequencies of 1.8 kHz and 15 kHz, respectively. The time scale has been normalized with respect to the true arrival time of the shear wave *Ta* as determined by analytical

solution. For low values of R_d there is an initial downward deflection of the trace before the shear wave arrives, representing the near-field effect. At high R_d the near-field effect is almost absent. To avoid it they proposed using a distorted sinus wave as input or alternatively using resonant frequency of the bender elements as input signal. (Brignoli et al., 1996) gave further evidences on the near-field effect. Figure 37 shows some typical waveforms with different frequencies. The input signal is a one-period-sinus. To the right of each record, the input and output frequencies are given, and the ratio d/λ, where d is the effective length, and λ is the wave length. This figure indicates that for low frequencies, the output signal tends to show previous arrival to that from higher frequencies. Another series of tests were done on dry silty clay supports their previous findings Figure 38. Three frequencies were used; 2.5, 5, and 10 kHz to show clear differences in arrivals.

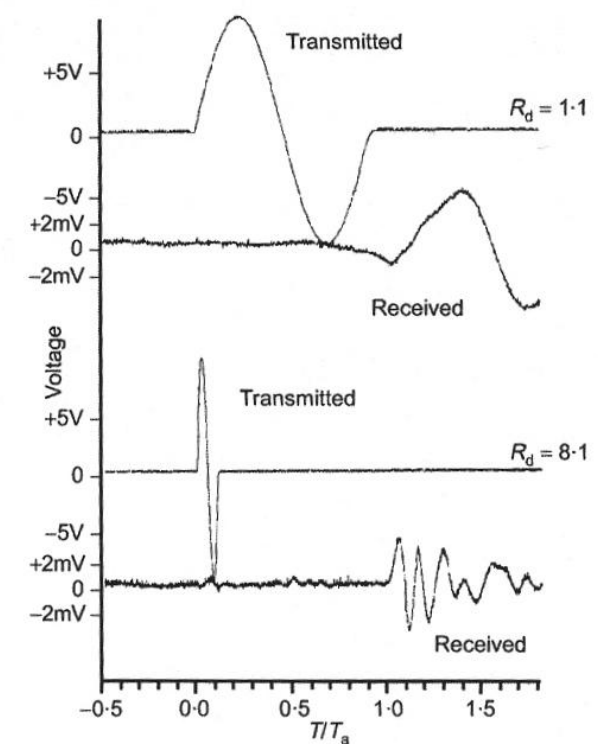

Figure 36. Test data with different R_d (Jovičić et al., 1996).

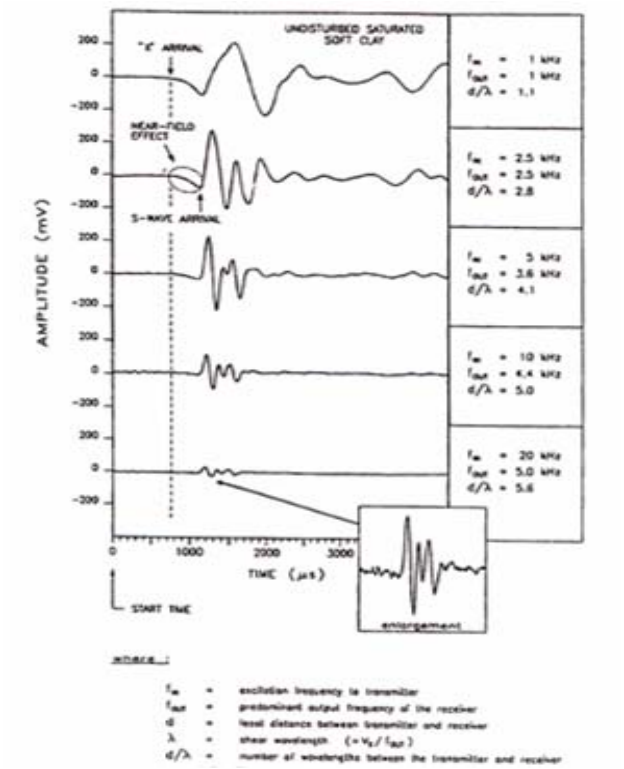

Figure 37. Waveforms with different frequencies (Brignoli et al., 1996).

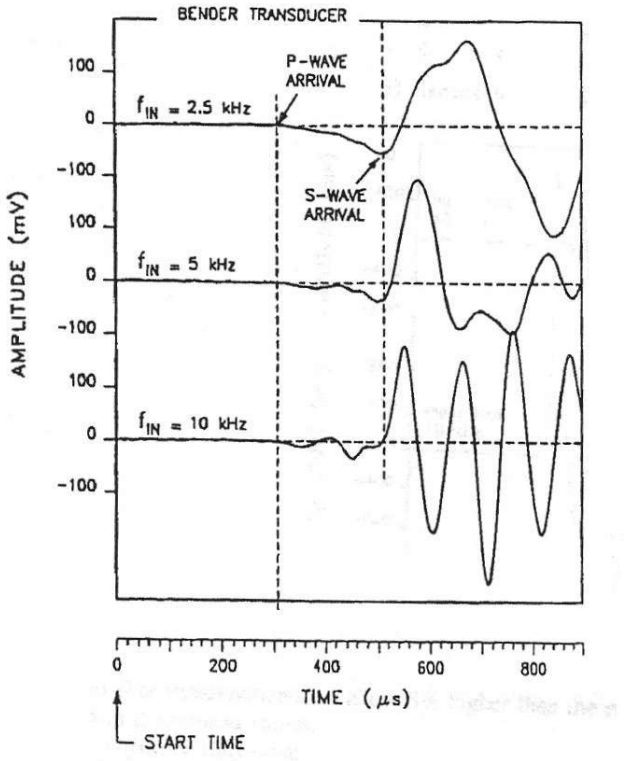

Figure 38. Differences in arrivals, f= 2.5, 5, and 10 kHz (Brignoli et al., 1996).

4.6.4 Different first arrivals

(Viggiani and Atkinson, 1995) compared different first arrival of the received signal at different potential points illustrated in Figure 39. Point A is the first deflection; point B in the first inflection; point C is the first zero after inflection; and point D is the second inflection. In their test using sample dimensions 38 mm in diameter and 76 mm in length in a triaxial cell, the travel time measured at point D was twice as the one measured at point A. This gives difference in calculated shear stiffness between these two points as high as 4 times. As a conclusion they recommended using frequency methods to determine the shear wave velocity. Table 3 shows their results on shear wave velocity from bender element test using different analysis methods at different arrival points which are illustrated in Figure 39. Figure 40 shows results of shear wave velocities at the previous different arrival points.

(Jovičić et al., 1996) proved the effect of the near-field experimentally and proposed using resonant frequency of the bender elements as input signal.

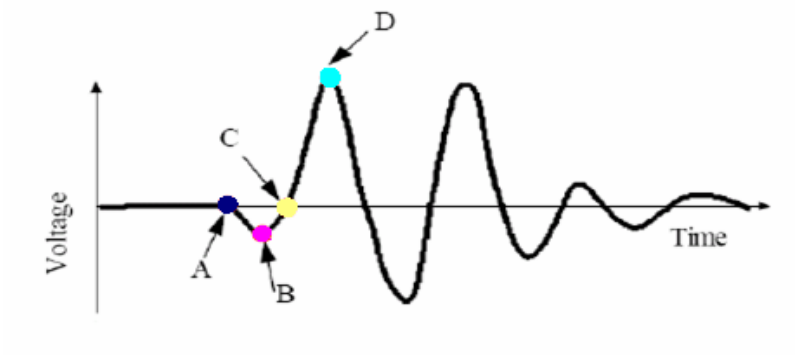

Figure 39. Potential arrival points.

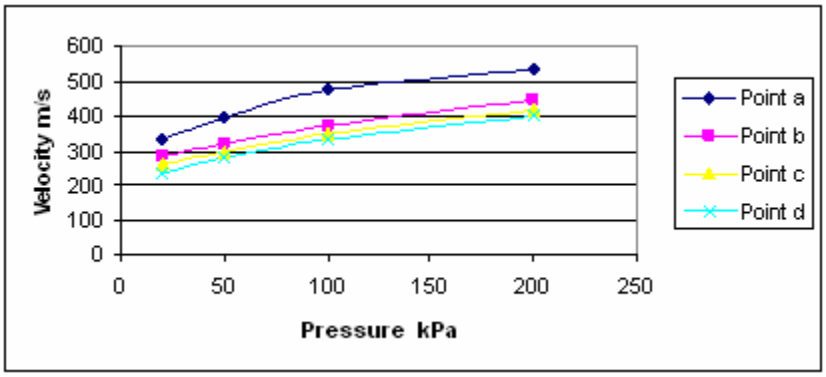

Figure 40. Shear wave velocity vs. pressure at different arrival points from Figure 39.

Table 3. Determination of shear wave velocity from bender element test using different analysis methods. Arrival points are illustrated in Figure 39. modified after (Viggiani and Atkinson, 1995).

Wave form	Analysis method	Arrival point	Travel time ms	Velocity m/s
Square wave	Selected points	A	0.280	250
		B	0.485	144
		D	0.564	124
Single sine wave	Peak to peak	A	0.493	142
		B	0.520	135
		D	0.533	133
	Cross correlation	0.524		134
	Cross-power spectrum	0.530		132

4.6.5 Comparison between bender elements and resonant column results

(Dyvik & Madshus, 1985) first installed bender elements in a resonant column device in order to measure in both tests simultaneously on five different clays. They found that G_{max} results from 10 to 150 MPa by both techniques were in excellent agreement (Figure 41).

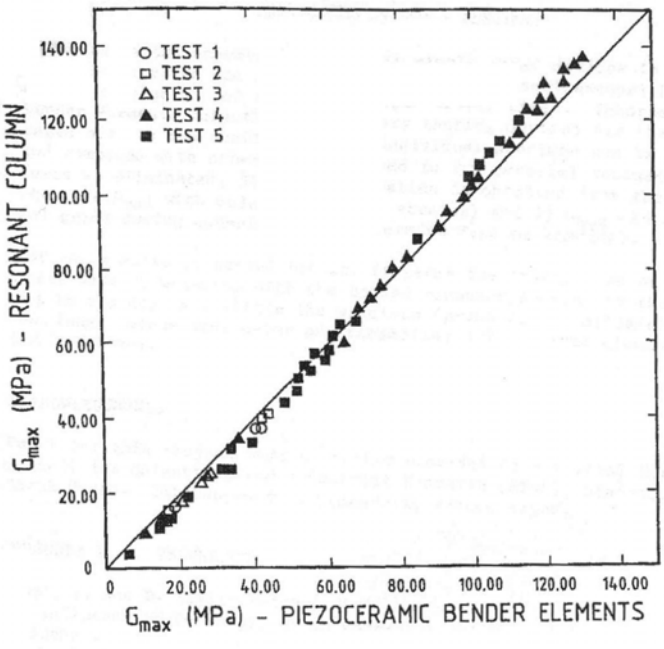

Figure 41. Comparison between G_{max} results by bender elements and resonant column tests (Dyvik & Madshus, 1985).

A recent study by (Ferreira et al., 2006) agrees with (Dyvik & Madshus, 1986). They interpreted the data of the bender elements test in two different methods; in time and frequency domain. The first arrival was used as time domain method and phase-delay method as frequency method. Figure 42 shows that the frequency domain results of G_{max} deviate from resonant column results by less than 1% in average, in the time domain, results of G_{max} are within an average of 2% of the resonant column values. (Brignoli et al., 1996) compared shear wave velocity for three soils using bender elements, shear plate and resonant column. By analyzing results in all three materials, they found that bender elements and resonant column compare well.

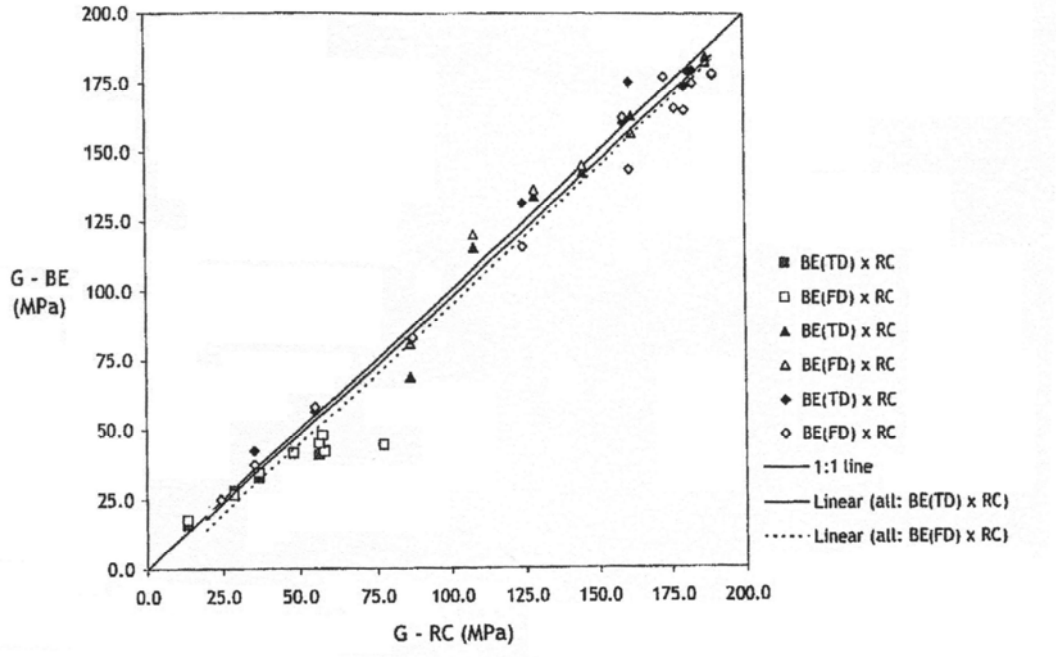

Figure 42. G_{max} determined with resonant column and bender elements. TD: time domain; FD: frequency domain (Ferreira et al., 2006).

(Youn et al., 2008) compared shear wave velocity obtained from bender elements, resonant column, and torsional shear on two sands in dry and saturated condition at various relative densities and effective confining pressures. In dry condition, values of shear wave velocity from bender elements and resonant column are in good agreement. In saturated condition, values of shear wave velocity determined with bender elements are greater than those of resonant column. Figure 43 shows variations in G_{max} with effective confining pressure obtained from bender elements (peak-to-peak method), resonant column and torsional shear tests for dry Silica sand. The G_{max} values from these three methods at confining pressures of 50,100, and 200 kPa show a maximum difference of about 3% relative to the mean value of each confining pressure stage.

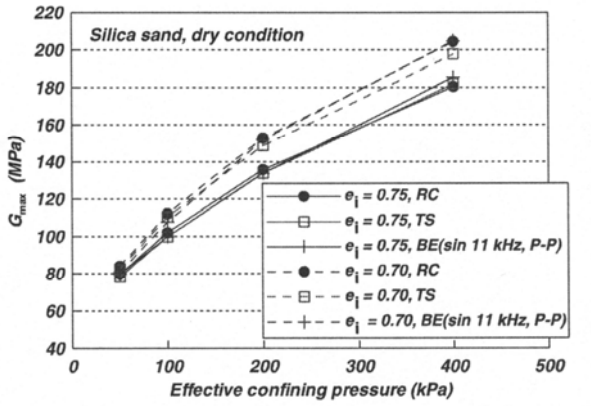

Figure 43. G_{max} versus effective confining pressure obtained from bender elements, resonant column and torsional shear tests for dry Silica sand (Youn et al., 2008).

4.6.6 Interpretation methods

Interpretation methods for results from bender elements test is briefly presented here. Further discussion about reliability, uncertainty and limits is shown in the next chapter.

First deflection

Considering the first deflection as the first arrival of the shear wave was very common in the beginning of the bender elements technique. This method of interpretation assumes plane wave fronts and the absence of any reflected or refracted waves. Travel time is calculated between the start of input signal (point A, Figure 44) and the first deflection from zero line (point C). This method completely ignores the near-field effect and P waves.

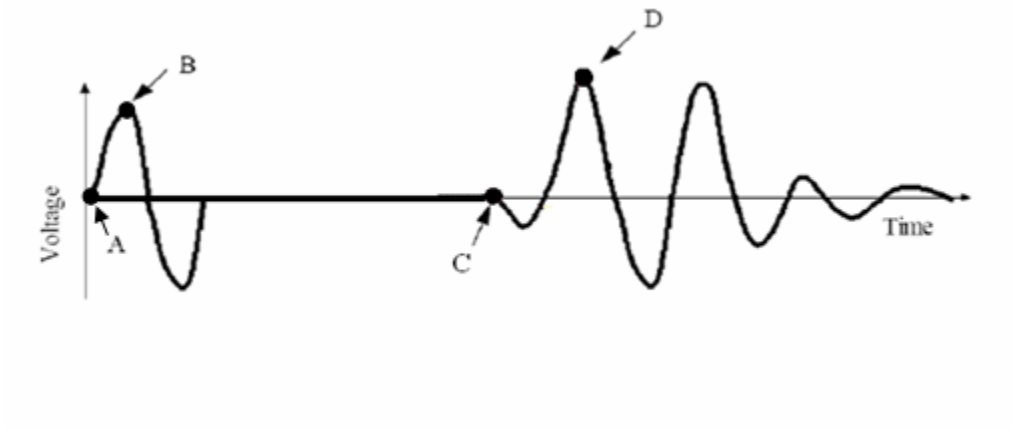

Figure 44. Characteristic points for interpretation methods.

Characteristic Peaks

This method assumes the travel time as the time between two Characteristic points in input and output or both in output in the case of the existence of a second arrival. In the first case, the peak of the input signal (point B, Figure 44) and the first peak in the output signal (point D). If two arrivals are received, measuring the time travel between two peaks or two troughs is possible (Figure 45).

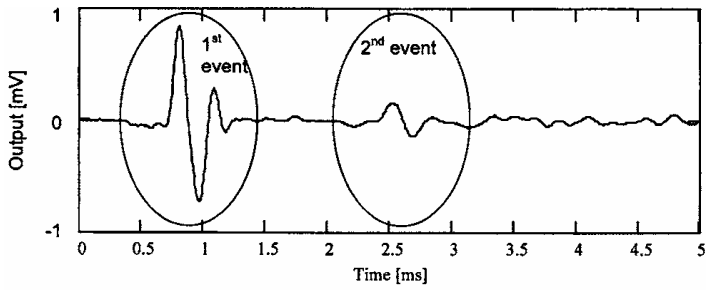

Figure 45. Two arrivals in output signal (Lee & Santamarina, 2005).

Cross-Correlation method

Travel time is taken as the time shift that produces the peak cross-correlation between signals recorded, based on the assumption of plane wave fronts and the absence of any reflected or refracted waves. For an impulse wave that has been recorded at two spaced points will reach maximum value for the time shift that equals the travel time of the impulse between two points. It is convenient to calculate cross-correlation in the frequency domain using the Fast Fourier Transform (FFT).

4.7 Summary

A number of different factors affect the measurements of G_{max} in the bender elements test. While measuring density and effective length look easy, determining travel time seems to be problematic due to many reasons like the near-field effect. Although there are many methods in the time and frequency domain to determine the travel time, the first arrival is the basic problem in this test, and it is still under discussion. Since there is no standard for this test, comparison between tests from different laboratories should be carefully done. Bender elements tests measurements showed good agreement with measurements from resonant frequency test. Concepts of interpretation methods are showed. Further discussion about uncertainty and limits of them is given in the next chapter.

Chapter V
Discussion and Future Work

G_{max} is a very important and critical parameter. The critical role of soil stiffness at small-strains in the design and analysis of geotechnical infrastructure is now widely accepted. Unfortunately, determining G_{max} is not an easy objective, due to the large number of factors affecting its value and its reduction curve. Although some of these factors have small influence, the others have a significant and complicated influence. Strain amplitude, void ratio and confining pressure seem to be the most important parameters that affect the small-strain stiffness of the soil. Table 1 shows a list of parameters that with different level of importance.

The in-situ tests are presented in this paper. Unfortunately, there is a number of disadvantages in these tests, such as showing the effects of just the current in-situ condition, requirement specialized costly equipments and complicated data interpretation. The accuracy of such tests is a critical point due to a variety of sources of errors (i.e. background noise, groundwater table effects). Laboratory tests give a good alternative possibility to measure G_{max} under different conditions. In the resonant column test, existence of error is possible, due to dependence on the resonant frequency of the soil-equipment system, specimen dimensions and mass (Dyvik & Madshus, 1985). A necessity for another laboratory method to easily determine small-strain stiffness is clear. The bender elements give such opportunity to measure shear wave velocity in soil using a simple concept. An advantage of this method is that the computation of Gmax is more direct and simple than other methods like the resonant column test or in-situ tests. Bender elements are easy to install into most soil testing apparatus (i.e., triaxial test, shear test, resonant column test and oedometer test). The bender elements themselves are cheap, small and lightweight, furthermore they are non-destructive.

Many researchers did verification for bender elements by comparing them with resonant column. Firstly, (Dyvik & Madshus, 1986) installed bender elements in a resonant column device in order to determine small-strain behaviour in both tests simultaneously on five different clays. They found that G_{max} results from 10 to 150 MPa by both techniques were in excellent agreement. This finding was supported by (e.g. Ferreira et al., 2006). (Brignoli et al., 1996) compared bender elements with resonant column in three soils. They found that shear wave velocity values determined with bender elements are slightly higher than values determined with resonant column. (Youn et al., 2008) compared shear wave velocity obtained from bender elements, resonant column, and torsional shear on two sands in dry and saturated condition. They found that G_{max} values from these three methods at confining pressures of 50,100, and 200 kPa show a maximum difference of about 3% relative to the mean value of each confining pressure stage.

In the international parallel test on the measurement of G_{max} using bender elements by Technical committee, TC29 (Stress-strain and Strength Testing of Geomaterials) of International Society of Soil Mechanics and Geotechnical Engineering (ISSMGE), evaluation of bender element test results from 23 institutions from 11 countries has been done, no clear influence of the difference in bender size, its structure,

cantilever length and wiring method was recognized. Therefore, further work should be done on this point, in order to determine the influence of these parameters, if any.

All technical properties of the bender elements should be exactly determined such as resonant frequency in air and in soil, frequency-amplitude relationship (transfer function), the influence of parallel and series connection and delay time. The later can be measured by putting both source and receiver bender elements with contact and measure the travel time between input and output signal. The source of this time delay is the reaction time of the bender elements and of the used hardware. Furthermore, installing bender elements in a cell without a specimen to make sure that the shear wave is not transferred through the cell frame (Schultheiss, 1981).

(Lee & Santamarina, 2005) found that the resonant frequency of bender element installations depends on the geometry of the bender element, the anchor efficiency and the soil stiffness. Effective stress can change bender elements characteristics like resonant frequency, (Schultheiss, 1981) and (Lee & Santamarina, 2006) because The resonant frequency of the bender element in soil is bender element stiffness dependent for short cantilever lengths, and it is soil stiffness dependent for long cantilever lengths, (Lee & Santamarina, 2005) . (Zeng & Ni, 1998) reported a great effect of the size of bender elements on results. They noticed that any change in sample size, distance between bender elements, or mounting technique will change the optimum size of bender elements.

The Technical committee, TC29 (Stress-strain and Strength Testing of Geomaterials) of International Society of Soil Mechanics and Geotechnical Engineering (ISSMGE) found that there is no clear effect of input frequency in case of the saturated samples but for dry specimens it seems that scatter is slightly on the higher side at lower frequencies. But these findings have no agreement with a lot of researchers such as (Brignoli et al., 1996; Jovičić et al., 1996; Sanchez-Salinero et at., 1986; and Lee & Santamarina, 2005) among others. This shows a lack which needs to be focused on in future work. This problem is probably associated with the basic problem of the near-field effect and technical properties of the bender elements themselves.

A variety of wave forms were used; sine wave, square wave, distorted sine wave, pulse, harmonic and sweep. The square wave contains a wide range of frequencies which strengthen the near-field effect, therefore it was recommended by many researchers to avoid using it and to use continuous signals because it increases the quality of results (Rio et al., 2003).

A numerical study presented by (Arroyo et al., 2006) and (Rio et al., 2003) has shown a clear size effect on the propagating signal due to reflections from the lateral boundaries of the sample. Very limited studies focused on the size effect of the sample and boundary reflection.

First arrival (for pulse signal) techniques give a systematically higher value of Vs and hence G_{max} relative to phase-delay methods Greening et al. (2003). Although the

near-field effect has a critical influence on the results, (Arroyo et al., 2003) found that near-field effects are not sufficient to explain the scatter observed in laboratory bender element measurements, and other factors should be involved. These difficulties in test interpretation have been noticed before, and various strategies for minimizing the error have been put forward. For example, (Brignoli et al., 1996) advocated simultaneous measurements with P-wave transducers. (Viggiani & Atkinson, 1995a) introduced frequency-domain- based methods of examining the test results. (Jovičić et al., 1996) suggested that time domain procedures may be adequate with a properly specified input signal. A common feature of these works was the identification of source near-field effects as the main cause of test uncertainty.

(Arulnathan et al., 1998) proved that interpretation methods using characteristic peaks or cross-correlation between the input and output signals are theoretically incorrect for a variety of reasons; wave interference at the boundaries, transfer function, and near-field and non-one-dimensional wave travel effects. Commenting on the recommendation of (Jovičić et al., 1996) that using a high value of d/λ minimizes the near-field effect, they argued that such a high value may result a value of wave length/bender length which is not optimal of maximizing signal strength.

As a conclusion of the previous discussion, the near-field effect has a critical influence on the results. First arrival method is significantly inaccurate. Avoiding the near-field effect by increasing the value of d/λ is useful but not sufficient. Other time domain methods like peak-to-peak or cross-correlation are proved to be also inaccurate. Isolating the near-field from the far field analytically (e.g. Arroyo et al., 2003) will be a meaningful procedure to evaluate the shear wave velocity in the far field.

A necessity for other methods rises, such as frequency domain methods. There are limited researchers worked on frequency domain methods (e.g. Greening & Nash, 2004) but there is no favorable specific one.

Bender elements test became widely used and improved in recent years. However, till now this test has not been standardized and many effects are not clear. The following ideas are worthy to be studied in future work:

- The critical influence of the near-field effect should be studied, and different ways to avoid it should be tried, such as applying different frequencies, different wave forms and different signal analysis in both time and frequency domain.

- Trying different methodologies in the frequency domain is useful to avoid uncertainty in time domain methods.

- Technical properties of bender elements must be quantified. The influence of the following parameters should be studied to improve the quality of the output

signal: bender elements size, bender elements structure, cantilever length, resonant frequency in air and in soil, frequency-amplitude relationship (i.e. transfer function), parallel and series connection and delay time.

- The influence of input frequency on shear wave velocity, and its relationship with the near-field effect.

- The influence of wave forms on shear wave velocity.

- The influence of sample size should be clarified.

- Taking into consideration the results and clarifications of the previous points, one can reevaluate the relationships between shear wave velocity and each of effective stress and void ratio.

References

[1] Anderson, D. G. and Stokoe, K. H. Shear modulus: A time-dependent soil property. *Dynamic Geotechnical Testing*, *ASTM STP654*, pp. 66-90, 1978.

[2] Arroyo, M., Muir Wood, D. and Greening, P. D. Source near-field effects and pulse tests in soil samples. *Géotechnique* 53, No. 3, pp. 337–345, 2003.

[3] Arroyo, M., Muir Wood, D., Greening, P. D., Medina, L. and Rio, J. Effects of sample size on bender-based axial G_0 measurements. *Géotechnique* 56, No. 1, pp. 39–52, 2006.

[4] Arulnathan, R., Boulanger R.W. and Riemer, M.F. Analysis of Bender Element Tests. *ASTM Geotechnical Testing Journal*, Vol. 21, No. 2, pp. 120-131, 1998.

[5] Atkinson, J.H. Non-linear soil stiffness in routine design. *Géotechnique* 5, No. 5, pp. 487–508, 2000.

[6] Atkinson, J.H. and Sallfors, G. Experimental determination of soil properties. *Proc. 10th Eur. Conf. Soil Mech., Florence 3*, 915-956, 1991.

[7] Benz, T. *Small-Strain Stiffness of Soils and its Numerical Consequences*. PhD thesis, University of Stuttgart, 2007.

[8] Biarez, J. and Hicher, P.-Y. *Elementary Mechanics of Soil Behaviour*. Balkema, 1994.

[9] Bishop, A. W. The principle of effective stress. *Teknisk Ukeblad I Samarbeide Med Teknikk*, Oslo, Norway, 106(39), pp. 859–863, 1959.

[10] Bishop, A. W. The measurement of pore pressure in the triaxial test. *Proc. Conference of British Nat. Soc. of Int. Soil Mechanics and Foundation Engineering*, Butterworth's, London, pp. 38–46, 1961.

[11] Bishop, A. W. and Blight, G. E. Some aspects of effective stress in saturated and partly saturated soils. *Géotechnique* 13, No. 3, pp. 177–196, 1963.

[12] Brignoli, E.G.M., Gotti, M. and Stokoe, K.H. Measurement of shear waves in laboratory specimens by means of piezoelectric transducers. *ASTM Geotechnical Testing Journal*, Vol. 19, No. 4, pp. 384–397, 1996.

[13] Burland, J.B. Small is beautiful - The stiffness of soils at small strains. *Canadian Geotechnical Journal*, 9th Laurits Bjerrum memorial lecture, 1989.

[14] Cho, G.-C.; Santamarina, J. C. Unsaturated particulate materials-Particle-level-study. *ASCE Journal of Geotechnical and Geoenvironmental Engineering*, Vol. 127, No. 1, pp. 84-96, 2001.

[15] Clayton, C. R. I . and Heymann, G. Stiffness of geomaterials at very small strains. *Géotechnique* 51, No. 3, pp. 245–255, 2001.

[16] Dobry, R. and Vucetic, M. State-of-the-art report: Dynamic properties and response of soft clay deposits. *Proc. Int. Symp. on Geotechnical Engineering of Soft Soils*, Vol. 2, pp. 51-87, 1987.

[17] Dyvik, R. and Madshus, C. Laboratory measurements of G_{max} using bender elements. *Proceeding ASCE Annual Convention: Advances in the art of testing soils under cyclic conditions*, pp. 186–196, 1985.

[18] EPRI. Guidelines for determination design basis ground motion. *Electric Power Research Institute*, Palo Alto, California, Vol. 1, pp. 8-1 through 8-69, 1993.

[19] Fernandez, A.l. and Santamarina, J.C. . Effect of cementation on the small-strain parameters of sands. *Canadian Geotechnical Journal*, Vol. 38, pp. 191-199, 2001.

[20] Ferreira, C., Santos, J.A. and Fonseca, A.V. Comparison of simultaneous bender elements and resonant column tests on Porto residual soil. *Geotechnical Symposium in Roma*, pp. 523-535, 2006.

[21] Fioravante, V. Anisotropy of small-strain stiffness of Ticino and Kenya sands from seismic wave propagation measured in triaxial testing. *Soils and Foundations*, Vol. 40, No. 4, pp. 129-142, 2000.

[22] Fredlund, D. G., Morgenstern, N. R. and Widger, R. A. The shear strength of unsaturated soils. *Canadian Geotechnical Journal*, Vol. 15, No. 3, pp. 313–321, 1978.

[23] Greening, P.D. and Nash, D.F.T. Frequency domain determination of G_0 using bender elements. *ASTM Geotechnical Testing Journal*, Vol. 27, No. 3, pp. 288-294, 2004.

[24] Greening, P.D., Nash, D.F.T., Benahmed, N., Ferreira, C. and. Viana da Fonseca, A. Comparison of shear wave velocity measurements in different materials using time and frequency domain techniques. *Deformation Characteristics of Geomaterials, Di Benedetto et al. (eds.)*, pp. 381-386, 2003.

[25] Hardin, B. O. The nature of stress-strain behavior for soils. *Proc. ASCE Geotech. Engrg. Div. Specialty Conf. on Earthquake Engineering and Soil Dynamics*, Vol. 1, pp. 3-90, 1978.

[26] Hardin, B.O. and Black, W.L. Vibration modulus of normally consolidated clays. *Proc. ASCE: Journal of the Soil Mechanics and Foundations Division*, 94(SM2), pp. 353-369, 1968.

[27] Hardin, B.O. and Drnevich, V.P. Shear modulus and damping in soils: Measurement and parameter effects. *Proc. ASCE: Journal of Soil Mechanics and Foundation Divisio*n, 98(SM6), pp. 603-624, 1972.

[28] Hardin, B.O. and Richart, F.E. Elastic wave velocities in granular soils. *Journal of Soil Mechanics and Foundations Division*, 89(SM1), pp. 33-65, 1963.

[29] Hicher, P.-Y. Elastic properties of soil. *ASCE Journal of Geotechnical Engineering*, 122(8), pp. 641-648, 1996.

[30] Hoque, E. and Tatsuoka, F. Effects of stress ratio on small-strain stiffness during triaxial shearing. *Géotechnique* 54, No. 7, pp. 429-439, 2004.

[31] Hsu, C-C. and Vucetic, M. Dynamic and cyclic behavior of soils over a wide range of shear strains in NGI-type simple shear testing device. UCLA Research Report ENG-02-228, Civil and Environmental Engineering Department, University of California, Los Angeles, 2002.

[32] Hynes-Griffin, M. E. *Pore pressure generation characteristics of gravel under undrained cyclic loading*. PhD thesis, University of California, Berkeley, 1988.

[33] Idriss, I. M., Dobry, R., Doyle, E. H. and Singh, R. D. Behavior of soft clays under earthquake loading conditions. *Proc. Eighth Annual Offshore Tech. Conf.*, pp. 605-616, 1976.

[34] International Society of Soil Mechanics and Geotechnical Engineering (ISSMGE). *International parallel test on the measurement of G_{max} using bender elements organized by TC-29*, 2007.

[35] Ishihara, K. Evaluation of soil properties for use in earthquake response analysis. *Geomechanical Modelling in Engineering Practice*, Dingar, R. and Studer, J. A. (eds.), A. Balkema, Rotterdam, the Netherlands, pp. 241-275, 1986.

[36] Ishihara, K., Huang, Y. and Tsuchiya, H. Liquefaction resistance of nearly saturated sand as correlated with longitudinal wave velocity. *International Conference Centrifuge 98*, Tokyo, 1998.

[37] Iwasaki, T. and Tatsuoka, F. Effects on grain size and grading on dynamics shear moduli of sands. *Soils and Foundations*, Vol. 17, No. 3, pp. 19-35, 1977.

[38] Jovičić, V., Coop, M.R. and Simić, M. Objective criteria determining G_{max} from bender elements tests. *Géotechnique* 46, No. 2, pp. 357-362, 1996.

[39] Kalliouglou, T.T. and Papadopoulou, A. Shear modulus and damping of natural sands. *Deformation Characteristics of Geomaterials, Di Benedetto et al*. (eds). pp. 401-407, 2003.

[40] Karl, L. *Dynamic Soil Properties out of SCPT and Bender Element Tests with Emphasis on Material Damping*. PhD thesis, Ghent University, 2005.

[41] Kim, T. C. and Novak, M. Dynamic properties of some cohesive soils of Ontario. *Canadian Geotechnical Journal*, Vol. 18, No. 3, pp. 371-389, 1981.

[42] Kokusho, T., Yoshida, Y. and Esashi, Y. Dynamic properties of soft clay for wide strain range. *Soils and Foundations*, Vol. 22, No. 4, pp. 1-18, 1982.

[43] Kramer, S. L. *Geotechnical Earthquake Engineering.* Prentice-Hall, 1996.

[44] Krautkrämer, J. and Krautkrämer, H. *Ultrasonic Testing of Materials*. 4th Edition, Springer, 1990.

[45] Kurup, P.U. Innovations in cone penetration testing. *Proc. of Sessions of GeoShanghai 2006*. China, June 6–8, pp. 48-55, 2006.

[46] Kuwano, R. and Jardine, R.J. On the application of cross-anisotropy elasticity to granular materials at very small strains. *Géotechnique* 52, No. 10, pp. 727-749, 2002.

[47] Lade P.V. and Abelev, V. Characterization of cross-anisotropic soil deposits from isotropic compression test. *Soils and Foundations*, 45(5), pp. 89-102, 2005.

[48] Lai, C.G., Rix, G.J., Foti, S. and Roma, V. Simultaneous measurement and inversion of surface wave dispersion and attenuation curves. *Soil Dynamics and Earthquake Engineering*, Vol. 22, No. 9-12, pp. 923-930, 2002.

[49] Lee, J.-S. and Santamarina, J.C. Discussion "Measuring shear wave velocity using bender elements" by Leong E. C., Yea, S. H. and Rahardjo, H. *Geotechnical Testing Journal,* Vol. 29, No. 5, pp. 439-441, 2006.

[50] Lee, J.-S. and Santamarina, J. C. Bender Elements: Performance and Signal Interpretation. *ASCE Journal of Geotechnical and Geoenvironmental Engineering*, Vol. 131, No. 9, pp. 1063-1070, 2005.

[51] Lionetto, F., Licciulli, A., Montagna, F. and Maffezzoli, A. Piezoceramics: an introductive guide to their practical applications. *Ceramurgia/Ceramica Acta (C+CA)*, Vol. 34, pp. 107-127, 2004.

[52] Lo Presti, D.C.F. and Jamiolkowski, M. Discussion: Estimate of elastic shear modulus in Holocene soil deposits. *Soils and Foundations*, Vol. 38 (1), pp. 263-265, 1998.

[53] Lo Presti, D.C.F., Pallara, O., Lancellotta, R., Armandi, M., and Maniscalco. R. Monotonic and cyclic loading behaviour of two sands at small strains. *ASTM Geotechnical Testing Journal*, Vol. 16, No. 4, pp. 409-424, 1993.

[54] Mair, R.J. Developments in geotechnical engineering research: application to tunnels and deep excavations. *Proceedings of institution of Civil Engineering, Civil Engineering,* pp. 27-41, 1993. Unwin Memorial Lecture, 1992.

[55] Marcuson, W. F., III. and Wahls, H. E. Time effects on the dynamic shear modulus of clays. *ASCE: Journal of Soil Mechanics and Foundation Divisio*n, 98(12), pp. 1359-1373, 1972.

[56] Marosi, K.T. and Hiltunen, D.R. Characterization of spectral analysis of surface waves shear wave velocity measurement uncertainty. *ASCE Journal of Geotechnical Engineering*, 130 (10), pp. 1034-1041, 2004.

[57] Matsui, T., Ohara, H. and Ito, T. Cyclic stress-strain history and shear characteristics of clay. *J. Geotech. Engrg. Div., ASCE*, 106(10), pp. 1101-1120, 1980.

[58] Mitchell, J.K. and Soga, K. *Fundamentals of Soil Behavior*. John Wiley & Sons, third edition, 2005.

[59] Murphy III, W.F., Winkler, K. and Kleinberg, R.L. Acoustic relaxation in sedimentary rocks: Dependence on grain contacts and fluid saturation. *Geophysics*, Vol. 51, pp. 757-766, 1986.

[60] Murphy, W.F., Winkler, K.W. and Kleinberg, R.L. Frame modulus reduction in sedimentary rocks: The effect of adsorption on grain contacts. *Geophysical Research Letters*, Vol. 11, No. 9, pp. 805-808, 1984.

[61] Narazian, S. and Stokoe, K.H. Use of spectral analysis of surface waves for determination of moduli and thickness of pavement systems. *Transportation Research Record 954*, Transportation Research board, Washington, D.C., 1983.

[62] Piezo systems Inc. *Introduction to Piezo Transducer*. www.piezo.com.

[63] Pihl, J., Hammarstroem, M., Ivansson, S. and Moren, P. *Crosshole Investigations - Results from Seismic Borehole Tomography.* Stripa Project Internal Report, 1986.

[64] Qian, X., Gray, D. H. and Woods, R. D. Resonant Column Tests on Partially Saturated Sands. *ASTM Geotechnical Testing Journal*. Vol. 14. No. 3. pp. 266-275, 1991.

[65] Resonance Publications, Inc**.** *Piezoelectric Phenomena*. www.resonancepub.com.

[66] Richart, F. E. Some effects of dynamic soil properties on soil-structure interaction. *Geotech. Engrg. Div., ASCE*, 101(12), pp. 1193-1240, 1975.

[67] Richart, F. E., Woods, R. D. and Hall, J. R. Jr. Vibrations of soils and foundation. *Prentice-Hall, Inc.*, Englewood Cliffs, N.J, 1970.

[68] Rio, J., Greening, P. and Medina, L. Influence of sample geometry on shear wave propagation using bender elements. *Deformation Characteristics of Geomaterials, Di Benedetto et al*. (eds). pp. 963-967, 2003.

[69] Robertson, P.K., Campanella, R.G., Gillespie, D. and Rice, A. Seismic CPT to measure in-site shear wave velocity. *In Measurement and Use of Shear Wave Velocity for Evaluating Dynamic Soil Properties*, ASCE, New York, pp. 18-34, 1985.

[70] Romo, M. P. and Jaime, A. Dynamic characteristics of some clays of the Mexico Valley and seismic response of the ground. *Technical Report, Apr., Institute de Ingenieria*, Mexico City, Mexico, 1986.

[71] Sanchez-Salinero, I., Roesset, J.M., Stokoe, K.H. Analytical studies of body wave propagation and attenuation. *Report GR 86-15*. University of Texas at Austin, 1986.

[72] Santos, J.A. and Gomes Correia, A. Reference threshold shear strain of soil. Its application to obtain an unique strain-dependent shear modulus curve for soil. *Proc. 15th International Conference on Soil Mechanics and Geotechnical Engineering*, Istanbul, Turkey, Vol. 1, pp. 267-270, 2001.

[73] Schmidt, H.-G. *Lectures of Soil Dynamics*. Bauhaus university, Weimar, 2000.

[74] Schmidt, H.-G. and Schlesinger, B. Windpark Klettwitz Gründung von Windkraftanlagen auf einer Tagebau-Hochkippe, Teil 2 – Seismische Messungen. *Ohde – Kolloquium, TU Dresden*, 2005.

[75] Schmidt, H.-G. and Wuttke, F. Seismische Standorterkundung für Anwendungen in der Geotechnik. *Messen in der Geotechnik*. TU Braunschweig, Heft 77, pp. 153-72, 2004.

[76] Schultheiss, P.J. Simultaneous measurement of P & S wave velocities during conventional laboratory testing procedures. *Marine Geotechnology*, Vol. 4, No. 4, pp. 343-367, 1981.

[77] Seed, H.B. and Idriss, I.M. Soil moduli and damping factors for dynamic response analysis. Report 70-10, EERC, Berkeley, CA, 1970.

[78] Sheriff, R.E. and Geldart, L.P. *Exploration Seismology*. Second edition, Cambridge university press, 1995.

[79] Shibuya, S., Mitachi, T., Yamashita, S., and Tanaka, H. Effect of sample disturbance on G_{max} of soils – a case study. In Shibuya, S., Mitachi, T., and Miura, S., editors, *Prefailure Deformation of Geomaterials*, Vol. 2, pp. 77-82. Baklema, 1995.

[80] Shibuya, S., Tatsuoka, F., Teachavorasinskun, S., Kong X.J., Abe, F., Kim Y.S. and Park, C.S. Elastic deformation properties of Geomaterials. *Soils and Foundations*, Vol.32, No.3, pp. 26-46, 1992.

[81] Shirley, D.J. An improved shear wave transducer. *Journal of Acoustical Society of America*, 63(5), pp. 1643-1645, 1978.

[82] Shirley, D.J. and Hampton, L.D. Shear-wave measurements in laboratory sediments. *Journal of Acoustical Society of America*, 63(2), pp. 607-613, 1978.

[83] Stokoe, K.H., Darendeli, M.B., Andrus, R.D. and Brown, L.T. Dynamic soil properties: laboratory, field and correlation studies. In *Proc. 2nd International Conference on Earthquake Geotechnical Engineering,* Vol. 3, pp. 811-845. Balkema, 1999.

[84] Stokoe K.H., Darendeli, M.B., Gilbert, R.B., Menq, F.-Y., and Choi, W.K. Development of a new family of normalized modulus reduction and material damping curves. *In International Workshop on Uncertainties in Nonlinear Soil Properties and their Impact on Modeling Dynamics Soil Response*, UC Berkeley, CA, 2004.

[85] Stokoe, K.H. and Santamarina, J.C. Seismic-wave-based testing in geotechnical engineering. *In GeoEng 2000: An International conference on Geotechnical and Geological Engineering*, Vol. 1, pp. 1490-1536, Melbourne, Australia, 2000.

[86] Stokoe, K.H., Wright, S.G., Bay, J.A. and Roesset, J.M. Characterization of geotechnical sites by SASW method. *Geophysical Characterization of Sites*, eds. Woods, R.D., Balkema, Netherlands, pp. 15-25, 1994.

[87] Tatsuoka, F. and Shibuya, S. Deformation characteristics of soil and rocks from field and laboratory tests. Keynote Lecture (Session No.1). *Proc. of the 9th Asian*

Regional Conference on Soil Mechanics and Foundation Engineering, Bangkok, Vol. 2, pp. 101–170, 1991.

[88] Tatsuoka, F., Lo Presti, D.C.F. and Kohata, Y. Deformation characteristics of soils and soft rocks under monotonic and cyclic loads and their relationships. SOA Report, *Proc. Of the third international conference on recent advanced in Geotechnical earthquake engineering and soil dynamics*, St Luois (Prakash eds.) Vol.2 pp. 851-879, 1995.

[89] Tatsuoka, F. Impacts on geotechnical engineering of several recent findings from laboratory stress-strain tests on geomaterials. *Department of Civil Engineering Mechanics*, Columbia University, 2000.

[90] Viggiani, G. and Atkinson, J.H. Interpretation of bender element tests. *Géotechnique 45*, No. 1, pp. 149-154, 1995a.

[91] Viggiani, G. and Atkinson, J.H. Stiffness of fine-grained soil at very small strains. *Géotechnique* 45, No. 2, pp. 249-265, 1995b.

[92] Vucetic, M. Normalized behavior of offshore clay under uniform cyclic loading. *Canadian Geotechnical Journal*, Vol. 25, No. 1, pp. 33-42, 1988

[93] Vucetic, M. Cyclic threshold shear strains in soils. *ASCE Journal of Geotechnical Engineering,* 120(12), pp. 2208-2228, 1994.

[94] Vucetic, M. and Dobry, R. Degradation of marine clays under cyclic loading. *ASCE Journal of Geotechnical Engineering*, 114(2), pp. 133-149, 1988.

[95] Vucetic, M. and Dobry, R. Effect of soil plasticity on cyclic response. *ASCE Journal of Geotechnical Engineering,* 117(1), pp. 89-107, 1991.

[96] Vucetic, M. and Tabata, K. Influence of soil type on the effect of strain rate on small-strain cyclic shear modulus. *Soils and Foundation*, Vol. 43, No. 5, pp. 161-173, 2003.

[97] Vucetic, M., Tabata, K. and Matesic, L. Effect of average straining rate on shear modulus at small cyclic strains. In Di Benedetto, H., Doanh, T., Geoffroy, H. and Sauzéat, C., editors, *Deformation Characteristics of Geomaterials*, pp. 321-328. Balkema, 2003.

[98] Winkler, K. and Nur, A. Pore fluids and seismic attenuation in rocks. *Geophysical Research Letters*, Vol. 6, No. 1, pp. 1-4, 1979.

[99] Woods, R.D. Field and laboratory determination of soil properties at low and high strains. *Proc. of second international conference on recent advances in*

geotechnical earthquake engineering and soil dynamics. St. Luos, MO, Vol. II, pp. 1727-1741, 1991.

[100] Yamashita, S., Kohata, Y., Kawaguchi, T. and Shibuya, S. International round-robin test organized by TC-29. Advanced laboratory stress-strain testing of Geomaterials, Tatsuoka, Shibuya and Kuwano (eds.). Balkema, 2001.

[101] Yong, R.N. and Japp, R.D. A flow law for clays in dynamics compression. In *Proc. Int. Symp. Wave Propagation and Dynamic Properties of Earth materials,* Albuquerque, N.M. University of New Mexico Press, 1967.

[102] Youn, J.-U., Choo, Y.-W. and Kim, D.-S. Measurement of small-strain shear modulus G_{max} of dry and saturated sands by bender element, resonant column, and torsional shear tests. *Canadian Geotechnical Journal,* Vol. 45, pp. 1426–1438, 2008.

[103] Zdravkovic, L. and Jardine, R.J. Some anisotropic stiffness characteristics of a silt under general stress conditions. *Géotechnique* 47, No. 3, pp. 407-437, 1997.

[104] Zeng, X. and Ni, B. Application of bender elements in measuring G_{max} of sand under K_0 condition. *Geotechnical Testing Journal,* Vol. 21, No. 3, pp. 251-263, 1998.